



Review Article

A review of the adsorption method for norfloxacin reduction from aqueous media



Paschal Enyinnaya Ohale^a, Chinenye Adaobi Igwegbe^{a,b,*}, Kingsley O. Iwuozor^{c,d,*}, Ebuka Chizitere Emenike^c, Christopher Chiedozi Obi^{a,e}, Andrzej Białowiec^b

^a Department of Chemical Engineering, Nnamdi Azikiwe University, P. M. B. 5025, Awka, Nigeria

^b Department of Applied Bioeconomy, Wrocław University of Environmental and Life Sciences, Poland

^c Department of Pure and Industrial Chemistry, Nnamdi Azikiwe University, P. M. B. 5025, Awka, Nigeria

^d Nigeria Sugar Institute, Ilorin, Nigeria

^e Department of Polymer Engineering, Nnamdi Azikiwe University, P.M.B. 5025, Awka 420218, Nigeria

REVIEW HIGHLIGHTS

- Graphene oxide/Metal organic framework based composite gave the highest NRFX adsorption capacities (Q_{max}) of 1114.8 mg/g.
- The NRFX adsorptive uptake was most described by Langmuir isotherm and pseudo-second order models.
- Knowledge gaps in column studies and used adsorbent disposal method were seen for norfloxacin removal.

ARTICLE INFO

Method name:

A review of the adsorption method for norfloxacin reduction from aqueous media

Keywords:

Norfloxacin
Adsorption
Ecotoxicology
Water pollution
Desorption
Kinetics

ABSTRACT

Norfloxacin (NRFX) is one of a class of antibiotics known as broad-spectrum fluoroquinolone antibiotic that is frequently used to treat infectious disorders in both animals and humans. NRFX is considered an emergent pharmaceutical contaminate. This review's objective is to evaluate empirical data on NRFX's removal from aqueous medium. The environmental danger of NRFX in the aquatic environment was validated by an initial ecotoxicological study. Graphene oxide/Metal Organic Framework (MOF) based composite, followed by Magnesium oxide/Chitosan/Graphene oxide composite gave the highest NRFX adsorption capacities (Q_{max}) of 1114.8 and 1000 mg/g, respectively. The main adsorption mechanisms for NRFX uptake include electrostatic interactions, H-bonds, π - π interactions, electron donor-acceptor interactions, hydrophobic interactions, and pore diffusion. The adsorptive uptake of NRFX were most suitably described by Langmuir isotherm and pseudo-second order implying adsorbate-to-adsorbent electron transfer on a monolayer surface. The thermodynamics of NRFX uptake is heavily dependent on the makeup of the adsorbent, and the selection of the eluent for desorption from the solid phase is equally important. There were detected knowledge gaps in column studies and adsorbent disposal method. There's great interest in scale-up and industrial applications of research results that will aid in management of water resources for sustainability.

* Corresponding authors.

E-mail addresses: ca.igwegbe@unizik.edu.ng, chinenyeigwegbe@upwr.edu.pl (C.A. Igwegbe), kingsleyiwuozor5@gmail.com (K.O. Iwuozor).

Social media: [@chinenyeigwegbe](https://twitter.com/chinenyeigwegbe) (C.A. Igwegbe)

<https://doi.org/10.1016/j.mex.2023.102180>

Received 9 November 2022; Accepted 10 April 2023

Available online 11 April 2023

2215-0161/© 2023 The Authors. Published by Elsevier B.V. This is an open access article under the CC BY-NC-ND license

(<http://creativecommons.org/licenses/by-nc-nd/4.0/>)

Specifications table

Subject area:	Environmental Science
More specific subject area:	Adsorption
Name of the reviewed methodology:	A review of the adsorption method for norfloxacin reduction from aqueous media
Keywords:	Norfloxacin; Adsorption; Ecotoxicology; Water pollution; Desorption; Kinetics
Resource availability:	Not applicable
Review question:	What was the maximum adsorption capacity (Q_e) obtained for norfloxacin uptake? What adsorbent gave the maximum Q_e for norfloxacin? Is the adsorption of norfloxacin a physically or chemically controlled process?

Method details

Introduction

A new class of contaminants, known as emerging contaminants (ECs), have been discovered in wastewater. These include pharmaceutical compounds, illicit drugs, surfactants, etc. [1,2]. Antibiotics are the most significant and widely detected ECs because they are the third most widely used drugs in contemporary medicine, reportedly, above six percent of general prescription drugs [3]. They are commonly used to treat certain diseases in humans, chickens, cattle, fish, swine, etc. Indiscriminate discharge of these drugs has increased their presence in the environment, with a consequential impact on aquatic life, triggering changes in their growth and survival [4,5]. In addition, they also aid bacterial resistance, posing serious human health and environmental concerns [2,6].

Norfloxacin (NRFX) is a class of fluoroquinolone antibiotic commonly employed to combat both Gram-positive and Gram-negative bacteria [2,7,8]. NRFX has been broadly used as human medication (typically for the treatment of prostatitis and urinary tract infections) and veterinary medicine [9]. The antibiotics are located in sewage, animal husbandry, and hospital wastewater treatment plants [9]. Indiscriminate discharge of NRFX has led to its detection in sediments and rivers [10]. A recent work by Feng, Wang [11] reported the presence of NRFX in sewage treatment plant (STP) effluents and surface water from various parts of the world. Their report [11] revealed that the range of NRFX concentrations in the surface water is 33–1150 ng/L, while that of STP effluents is 9.4–170 ng/L.

Since the majority of conventional wastewater treatment facilities are not equipped to remove antibiotics, hence post-treatment effluent can release a sizable proportion of these NRFX-contaminated effluents into water bodies or the environment [5]. As a result, the removal of NRFX from aqueous solutions has gained the attention of researchers, particularly those in the field of the aquatic environment.

Several wastewater treatment methods have been investigated for the degradation/removal of NRFX from wastewater such as adsorption [1,4,6,7,9,12–18], membrane filtration [19], adsorption-photocatalytic [20], coagulation [21], electrocoagulation [22–24], photo-Fenton [25], electro-Fenton [26], photocatalyst [27], sonocatalytic [28], etc. The membrane separation method is costly and susceptible to fouling [18]. Photocatalytic and catalytic methods degrade antibiotics by breaking them down into small molecules. The high cost of catalysts limits their applications in large-scale operations and the identification of the noxiousness of the catalytic by-products is challenging [9]. Amongst these alternatives, adsorption is the most attractive technique in terms of economic viability [3,5]. Other advantages of adsorption over other alternatives in the removal of antibiotics from aqueous solutions include operational simplicity, high removal efficiency, applicability in a large sorbate concentration range, instrumentation cost benefit, etc., [4,13].

These promising attributes of adsorption towards the removal of antibiotics, in particular NRFX, from aqueous media, make it necessary to present a structured and comprehensive review of the recent research output in this area. The authors observed via painstaking research that despite years of studies in this area, there hasn't been a systematic review specifically focused on the adsorption of NRFX from aquatic solutions. NRFX was selected as the target pollutant for this study because of its wide usage in human and veterinary medicines making it highly detectable in the environment.

Hence, the focus of the present review is to comprehensively present, discuss, and summarize the research findings related to the adsorption of NRFX from an aqueous solution. The adsorbent materials with their respective adsorption capacities and the adsorption types, kinetics, isotherms, mechanisms, as well as thermodynamic equilibrium were elaborately analyzed. More so, the desorption/reusability capabilities of the individual adsorbents for NRFX sorption were discussed in detail. The review equally provided insight into main empirical research outcomes, identify research gaps and establish future research perspectives in the NRFX adsorption research arena. The papers published in the last decade were central to the review and the papers were all selected from the pool of reputable indexed journals.

Ecotoxicology of NRFX

When the concentration of NRFX in the aquatic environment grows beyond the allowable limit, it becomes an environmental challenge and a threat to aquatic life. This section briefly provides insight into the adverse impacts of the NRFX contamination of the aquatic environment. This provides legitimate justification for the imperativeness of NRFX removal from aqueous media. The properties and the chemical structure of NRFX are presented in Table 1 and Fig. 1 respectively. The changes in the growth and survival of aquatic habitats triggered by sole NRFX accumulation or its combination with other pollution agents have been highlighted.

The effect of NRFX contamination was investigated via co-culturing of *Scenedesmus quadricauda-Chlorella vulgaris* (SQCV) and *Scenedesmus obliquus-Chlorella vulgaris* (SOCV) in a short term and SOCV in a long term [29]. Their findings showed that NRFX impacted the interaction of species and reduced the stability over time of plankton communities, signifying that antibiotics such as

Table 1
Properties of NRFX [2,5,33].

Property	NRFX
Appearance CAS ID	crystalline powder (white to light-yellow) 70,458–96–7
IUPAC Name	1-Ethyl-6-fluoro-4-oxo-7-piperazin-1-ylquinoline-3-carboxylic acid
Chemical Formula	$C_{16}H_{18}FN_3O_3$
Composition (%)	C (60.18), H (5.68), F (5.95), N (13.16), O (15.03)
Molecular weight (g/mol)	319.33
Exact molar mass (g/mol)	319.13321961
Polar surface area (\AA^2)	72.9
Water Solubility (at 25 °C, pH = 7)	400 mg/L
λ_{max} /nm	278
pKa (Dual)	6.22 and 8.51
Heavy atom count	23
Molecular dimensions, size (\AA)	L12.2 \AA ×W8.2 \AA ×H7.0 \AA
Log K_{ow}	1.03
H ₂ bond count (Donor)	2
H ₂ bond count (Acceptor)	7
Melting point	220 – 221 °C

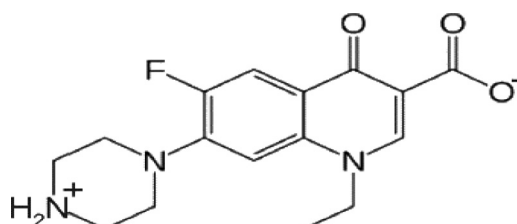


Fig. 1. Chemical structure of NRFX (Adopted from [2]).

NRFX have broader effects than currently understood. Wan, Long [30] demonstrated the impact of NRFX contamination on the aquatic food chain. Dual food chains, that is, *Chlorella vulgaris*-*D. magna*-larval and *Scenedesmus quadricauda*-*D. magna*-larval damselfly was used to study the impact of the presence (at different concentrations) of NRFX on trophic cascades. An increase in the concentration of NRFX triggered a reduction in the swimming capability of the species. Exposure to NRFX changed the trophic cascades' power and direction, and it revealed the specific variations of the species. Another study was conducted to determine the toxicity of NRFX towards *Lactuca sativa* via the estimation of the EC₅₀ (5 days), that is, the effective concentration that would give a root elongation inhibition of 50% in 5 days [30]. As the concentration of NRFX increases, there is a reduction in the seeds' ability to elongate their roots, hence, the samples' toxicity is raised. At up to 200 mg L⁻¹ NRFX concentration, the samples did not show toxicity, but from 350 mg L⁻¹ concentration, toxicity was demonstrated. Without a supporting electrolyte, the EC₅₀ (5 days) for an NRFX-contaminated solution was recorded as 336 mg L⁻¹. Corresponding results were obtained in a related study by Pan, Yan [31] using *Daphnia magna*. On the hand, studies showed that Norfloxacin nicotinate is immunotoxic and is toxic and hazardous to the formative stages of the life of zebrafish [32]. These reports demonstrate the imperativeness of studies directed towards the effective removal of NRFX from aqueous media.

Overview of NRFX removal methods

This section presents an overview of the different NRFX removal methods. This helps to provide insight into the capabilities and the advantages of adsorption over the other NRFX removal methods, further lending credibility to why the adsorption method was considered for this review. From the literature, the methods that have been investigated for the removal of NRFX from aqueous solutions can be grouped into three, viz, physical, chemical, and biological methods.

The physical methods comprise of microfiltration [34], ultrafiltration [35], and nanofiltration [19,36] membranes, reverse osmosis [36], and adsorption [6,9,12,14]. In the membrane filtration techniques, semipermeable materials are used to remove a pollutant from the contaminated effluent [38]. Nanofiltration and reverse osmosis have demonstrated the most separation capabilities, delivering $\alpha > 99\%$ NRFX removal at a pH of 8 [36]. Similarly, exactly 99.5% of NRFX were successfully removed from NRFX-contaminated pharmaceutical wastewater at a pH of 6.5 [19]. However, the membrane filtration technique is constrained by high installation and operating costs, and fouling susceptibility [37–39].

The chemical methods that have been reported include the coagulation-flocculation (C-F) [21], electrocoagulation (EC) [22], ion exchange [40], and advanced oxidation processes (AOPs) [41–44]. AOPs are unconventional techniques for repollutants degradation, they benefit from the high oxidation capability of hydroxyl radical ($\bullet\text{OH}$), azide radical ($\bullet\text{N}_3$), and sulfate radicals ($\text{SO}_4^{\bullet-}$) produced during the treatment process [38,45] to give inert end products. The efficacy of the oxidant determines how well AOPs perform [45]. AOPs investigated for NRFX removal include photocatalysis [27,46–48], photolysis [49,50], chlorine processes [51–53], ozonolysis

[54–56], sonolysis [57], sonocatalysis [28,58], Fenton (sono-Fenton, electro-Fenton, and photo-Fenton, etc.) [25,59–62]. The degradation of NRFX photolysis enhanced by microwave has been demonstrated by Liao, Sharma [49]. Within five minutes of the MW/UV reaction, approximately 75% of NRFX was removed. The NRFX degradation was chiefly initiated by ·OH-photosensitization stages and a second-order reaction kinetics was followed. Novel FeVO₄/Fe₂TiO₅-type composite photocatalyst was hydrothermally synthesized for NRFX degradation [46]. The novel photocatalyst irradiated with visible light exhibited enhanced photocatalytic activity and impressive stability during the treatment process. A study by Zhao, Wang [61] demonstrated a photo-Fenton NRFX degradation process via the immobilization of MIL-101(Fe)-NH₂ on Al₂O₃. The prepared photo-Fenton catalyst delivered a > 90% NRFX removal efficiency which was attributed to its outstanding water and chemical stability.

In a coagulation-flocculation process, anionic polyacrylamide and polyaluminium chloride were used as coagulants according to He, Zhang [21]. The process could only deliver an NRFX removal efficiency of about 42%. The process was reported to be predominantly controlled by sweep flocculation, surface charge neutralization, and adsorption. In a similar study, the performance of electrocoagulation in NRFX degradation was demonstrated using six aluminum electrodes arranged in parallel [22]. The process variables were electrocoagulation reaction time, solution pH, and operating voltage. At optimal conditions, a 98.4% NRFX removal was achieved. Nonetheless, most of these chemical methods have some identified shortfalls. For instance, the AOPs are associated with high cost of chemical reagents, energy, and operation, it can also lead to the generation of unknown side products [63]. The ion exchange method would require a buffer, the acidity of the solution is raised, it also require high operating cost [37]. The coagulation-flocculation method is constrained by high effluent sludge volume and possibility of use of environmentally unsafe chemicals as coagulants [63,64]. The electrocoagulation is associated with high electricity and electrodes costs, passivation of the sacrificial electrodes, and the need for further treatment to eliminate the raised metal concentration brought about by the dissolution of the metal electrodes used [65–68].

In biological methods, cultures of microorganisms are used to decompose contaminants [37]. Biological wastewater treatment is grouped into aerobic and anaerobic bioprocesses. Nitrogenous and organic components in the effluent can serve as nutrients for enhanced microbial proliferation in anaerobic or aerobic environments [37]. The performance of aerobic and anaerobic degradation techniques was reported by de Souza Santos, Teixeira [69]. The study revealed that NRFX degradation efficiency of 12% and 18% were obtained for activated sludge and anaerobic bio-digesters, respectively. The efficacy of microbial fuel cells for NRFX removal from aqueous media has also been investigated by Ondon and co-workers [70]. The NRFX removal efficiency of 65.5% was reported. As reported, raising the concentration of NRFX (up to 128 mg/L) had no substantial effect on its degradation efficiency. In an enzyme-based-activated sludge for NRFX degradation study, a degradation efficiency of 82.18% was obtained after 25 min, pH 5.0, and enzyme concentration of 1.5×10^{-9} mol L⁻¹ [71]. In another study, a high NRFX degradation efficiency via a bio-aerated filter incorporated with zeolite filler was demonstrated [72]. The degradation efficiency of NRFX was > 99.9%. The shortcomings of biological methods include the reality of requiring a longer time to complete the process, slow process kinetics, complexity of the microbiological process, and some compounds are not biodegradable or poor in biodegradability [37,63].

The adsorption method of pollutants removal is one of the most widely researched areas [73,74] due to its numerous advantages over other alternative methods including, equipment simplicity and ease of operation, low operating cost, high pollutant removal efficiency, ease of process combination with other methods, etc. [37,63,75,76]. It also has the advantage of the use of widely available waste materials and biomass which are considered worthless as adsorbents in the adsorption process [38]. Numerous adsorbent materials have been investigated for adsorptive removal of NRFX from aqueous media, they include carbon-based adsorbents [3,16,77,78], polymers [79–81], clays [10,82], composites [2,83,84], nano-materials [6,9,13,18], magnetic materials [85,86], etc. It is on the premise of the wide availability of research on NRFX adsorption that this review was conceived.

Adsorbent performance for NRFX

This section discusses the performance of various adsorbents for NRFX sequestration, as well as the various factors affecting their performance. Studies on NRFX adsorption have shown the use of removal efficiency (RE%) and maximum adsorption capacity (Q_{max}) as indexes for the representation of the adsorbent's performance. For two reasons, this study utilized only the maximum adsorption capacity as its index. Firstly, while all studies on NRFX adsorption reported the strength of the adsorbent based on its adsorption capacity, not all studies reported the same for the removal efficiency. Secondly, previous studies have shown that the choice of operational parameters greatly affects the RE% [87,88]. For most of the studies performed, the Q_{max} of the adsorbents was obtained through Langmuir isotherm modeling. However, some exceptions exist, such as experiments [89,90], and other isotherm modeling such as Sips [5,17], and Dubinin-Astakhov [91]. This implies that the adsorption of NRFX mostly occurred on the monolayer surface of the adsorbent. Table 2 summarizes the findings of various researchers on the uptake of NRFX using the adsorption technique. From the table, it can be observed that the adsorbents with the highest Q_{max} value for NRFX uptake are Graphene oxide/Metal Organic Framework (MOF) based composites, followed by Magnesium oxide/Chitosan/Graphene oxide composites, with NRFX adsorption capacities of 1114.8 mg/g [83], and 1000 mg/g [92], respectively. These adsorbents fall into the class of composite-based adsorbents as buttressed by Ighalo, Omoarukhe [93]. Apart from having high adsorption capacity, composite-based adsorbents were also observed to be the most frequently used adsorbents for NRFX uptake. The perceived high performance of composite-based adsorbents could be due to the contribution of the individual chemical constituents inherent in them [94].

The adsorbent's attributes or properties are one very important factor that affects its Q_{max} potential. These attributes can be divided into two types: physical and chemical properties. Examples of the adsorbent's physical attributes include its specific surface area, pore volume, and pore size [95–97]. To drive home this point, Zanli, Tang [98] varied the reaction conditions for the synthesis of cocoa shell-based biochar, which also caused a variation in the biochar's SSA, average pore diameter, and pore volume. The variation

Table 2
Adsorbent performance for NRFX adsorption from aqueous media.

Adsorbent	Q_{max} (mg/g)	pH	Temp. (°C)	SSA (m ² /g)	Average pore volume (cm ³ /g)	Method of q_{max} determination	Refs.
Graphene oxide/MOF based composite	1114.8	–	–	49.95	–	Langmuir	[83]
Magnesium oxide/Chitosan/Graphene oxide	1000.0	7.0	–	294.0	–	Langmuir	[92]
N-doped activated carbon from shaddock peel	798.40	–	45	2481	–	Langmuir	[102]
<i>Trapa natans</i> husk based AC	638.60	7.5	–	1274	1.087	Langmuir	[107]
Chitosan-hydroxyapatite nano-adsorbent	625.00	7.0	45	–	–	Langmuir	[6]
Pine needle based Fe/Cu oxides composite	609.86	–	40	27.80	0.093	Langmuir	[108]
Magnetic halloysite nanotubes/molecularly imprinted polymer composite	512.82	–	25	–	–	Langmuir	[109]
Lotus stalk-based activated carbon	456.18	5.5	–	1289	–	Langmuir	[110]
Fe-Cu oxide nanocomposite from Loquat leaf extract	453.70	–	40	13.38	0.055	Langmuir	[103]
Loofah based activated carbon	450.45	7.0	25	736.8	–	Experiments	[89]
Pre-treated barley straw	441.00	6.96	50	–	–	Experiments	[90]
Chromium based sulphonated MOF	408.20	7.0	30	1760	–	Langmuir	[99]
Pre-treated barley straw	396.00	7.0	25	1314	–	Experiments	[111]
Graphene oxide	374.90	7.0	31	67.00	–	Sips	[17]
Chromium based metal-organic framework (MOF)	360.00	–	30	–	–	Experiments	[99]
Raw barley straw	349.00	6.96	25	–	–	Experiments	[90]
Polydopamine microspheres	346.00	6.6	45	–	–	Langmuir	[80]
Iron-trimesic metal-organic framework	344.80	7.0	25	563.6	–	Experiments	[112]
Cattail fibres based activated carbon	310.70	–	–	907.0	1.00	Langmuir	[113]
Magnetic biochar derived from furfural residue	299.60	4.0	–	463.0	0.524	Langmuir	[114]
Amine-functionalized magnetic bamboo-based AC	293.20	–	–	923.2	0.51	Langmuir	[33]
<i>Luffa</i> sponge biochar	286.00	–	15	822.3	–	Langmuir	[3]
Animal hairs based activated carbon	285.40	–	–	514.0	0.243	Langmuir	[113]
Layered chalcogenide	271.10	4.0	40	–	–	Langmuir	[115]
Raw montmorillonite	255.44	5.0	25	–	–	Langmuir	[116]
Zr-based metal organic framework composite	253.16	–	–	–	–	Langmuir	[117]
3D peanut shell/graphene oxide	228.83	6.2	–	64.24	0.108	Experiments	[118]
Amino-functionalized Zr-based MOF	222.50	–	45	713.2	–	Langmuir	[9]
Surface-imprinted polymer microsphere	220.30	–	25	–	–	Langmuir	[119]
<i>Salix mongolica</i> based magnetic biochar	215.80	–	35	1348	0.59	Langmuir	[120]
Hypercross linked resin MN-202	196.10	7.0	45	1155	–	Langmuir	[121]
Alkali-modified fly ash	189.40	7.0	25	31.27	0.0773	Langmuir	[122]
Macroporous resin XAD-4	178.60	7.0	15	880.0	–	Langmuir	[121]
Magnetic bamboo-based AC	173.30	–	–	861.6	0.45	Langmuir	[33]
Montmorillonite	169.22	7.0	25	65.50	–	Langmuir	[2]
Aminated polystyrene resin MN-150	161.30	7.0	45	815.3	–	Langmuir	[121]
<i>Albizia lebbek</i> seed pods based activated carbon	153.99	–	50	1824	–	Langmuir	[123]
Iron-based mesoporous material (Fe-MCM-41)	134.26	–	–	894.1	–	Langmuir	[101]
Acid-modified fly ash	129.70	7.0	25	18.37	0.0403	Langmuir	[122]
Urea N-doped cocoa shell biochar	120.30	–	25	8.450	0.016	Langmuir	[98]
Granular AC	112.86	7.0	25	1200	1.31	Langmuir	[124]
Nitrogen rich-modified <i>Calotropis gigantean</i> fiber	105.80	8.0	–	–	–	Langmuir	[125]
Sulphuric acid activated termite feces	104.40	–	55	81.30	–	Sips	[5]
Diammonium hydrogen orthophosphate activated Pomelo peel based AC	101.35	–	30	83.79	0.08	Langmuir	[126]
Mg/Fe layered bimetallic hydroxides	97.070	7.0	25	–	–	Experiments	[127]
Thermally treated montmorillonite	95.790	7.0	25	1.200	–	Langmuir	[2]
Chromium based aminated MOF	92.500	–	30	–	–	Experiments	[99]
Carboxylated multi-walled carbon nanotubes	89.300	7.0	45	160.0	–	Langmuir	[121]
Copper loaded SBA-15 type mesoporous silica	87.850	–	35	–	–	Langmuir	[128]
Acid activated, thermally treated montmorillonite	86.211	7.0	25	131.6	–	Langmuir	[2]
Magnetic pomelo peel-based biochar	85.080	–	45	20.73	0.110	Langmuir	[104]
Spent coffee ground biochar	69.800	7.0	–	46.32	–	Langmuir	[129]
Magnetic porous carbon from Fe ³⁺ -modified MOF-5	63.918	7.0	25	104.0	0.24	Dubinin-Astakhov	[91]
Molecularly imprinted polymer	62.500	–	–	7.950	0.34	Langmuir	[81]
MCM-41type mesoporous silica	61.400	7.0	–	–	–	Experiments	[130]
Fly ash	54.690	7.0	25	6.120	0.0233	Langmuir	[122]
2D copper-porphyrin metal-organic framework	50.000	5.0	–	342.7	0.256	Experiments	[131]
Iron loaded SBA-15 type mesoporous silica	46.720	–	15	–	–	Langmuir	[128]
Pomelo peel-based biochar	45.270	–	45	1.706	0.003	Langmuir	[104]
Molecularly non-imprinted polymer	44.600	–	–	5.850	0.29	Langmuir	[81]
Magnetic molecularly imprinted polymer composite	42.340	–	35	–	–	Experiments	[132]
Sawdust biochar/Al ₂ (SO ₄) ₃ -modified thermal kaolin	42.287	–	–	44.00	0.233	Langmuir	[1]
Iron/Zinc/H ₃ PO ₄ – modified sludge biochar	39.300	–	–	39.10	0.129	Langmuir	[133]
Phosphoric acid activated Pomelo peel based AC	38.340	–	30	626.9	0.35	Langmuir	[126]

(continued on next page)

Table 2 (continued)

Adsorbent	Q_{max} (mg/g)	pH	Temp. (°C)	SSA (m ² /g)	Average pore volume (cm ³ /g)	Method of q_{max} determination	Refs.
Coffee husk waste	33.560	–	–	1.217	–	Langmuir	[16]
Iron-doped activated alumina	32.580	6.5	–	140.6	–	Langmuir	[110]
Montmorillonite/wheat straw biochar composite	25.530	7.0	25	112.6	0.604	Langmuir	[100]
Reduced graphene oxide/ magnetite composite	23.260	6.2	25	–	–	Langmuir	[134]
Rice husk waste	20.120	–	–	0.902	–	Langmuir	[16]
Magnetic molecularly imprinted polymer	14.260	–	25	88.90	0.15	Langmuir	[85]
Iron ore waste	14.160	–	35	24.60	–	Langmuir	[15]
Nickel-Aluminium layered double hydroxide	12.990	7.0	25	60.83	0.099	Langmuir	[34]
Urea N-doped biochar	11.480	5.0	25	225.9	0.24	Experiments	[135]
Wheat straw biochar	10.580	7.0	25	20.10	0.138	Langmuir	[100]
Magnesium-aluminum layered double hydroxides	9.0660	–	–	37.30	–	Experiments	[136]
Pomelo peel-based biochar	7.4300	4.5	20	–	–	Experiments	[137]
Corn stalks based activated magnetic biochar	7.2469	–	–	760.7	0.3698	Langmuir	[78]
Magnetic potato stems and leaves biochar-based manganese oxide composite	6.9400	3.0	35	252.0	0.16	Langmuir	[138]
Willow branches activated magnetic biochar	6.2587	–	–	856.8	0.4007	Langmuir	[78]
Pyrite-reed straw biochar composite	5.9425	7.0	35	54.53	0.0532	Langmuir	[139]
Potato stems and leaves biochar	5.8200	3.0	53	99.43	0.078	Langmuir	[138]
Natural attapulgite – potato stem hybrid biochar	5.2400	6.1	35	90.40	0.1225	Langmuir	[10]
Hematite-reed straw biochar composite	4.4699	7.0	35	134.9	0.0857	Langmuir	[139]
Reed stalks based activated magnetic biochar	3.5139	–	–	777.5	0.3294	Langmuir	[78]
Montmorillonite	2.5530	6.5	25	148.3	0.202	Experiments	[100]
Molecularly imprinted silica polymer	2.2280	–	25	344.0	–	Experiments	[140]
Carbonized <i>Moringa oleifera</i> pod husks	2.0330	–	25	235.8	–	Langmuir	[141]
Mesoporous silica MCM-41	1.7400	7.0	25	918.4	0.752	Langmuir	[142]
Chemically treated <i>Moringa oleifera</i> pod husks	1.5170	–	25	182.4	–	Langmuir	[141]
Polystyrene microplastics	0.9240	–	35	–	–	Langmuir	[7]
Polybutylene succinate	0.8340	–	35	–	–	Langmuir	[7]
Polyethylene microplastics	0.5140	–	35	–	–	Langmuir	[7]

in these attributes was also observed to contribute to the variation in the uptake ability of NRFX. The chemical attributes of the adsorbent are another factor that affects its performance. A study by Guo, Kang [99] showed that the addition of an amine functional group to a chromium-based MOF decreased its adsorption capacity for NRFX from 360 mg/g to 92.5 mg/g, while the addition of a sulphonic acid functional group improved its adsorption capacity to 400.9 mg/g. pH is another sensitive parameter that affects the performance of the adsorbent. The pH at which maximum adsorption of NRFX was obtained varied from 3.0 to 8.0, with most of it falling within the range of 6–7, as shown in Table 2. Norfloxacin has two proton-binding sites, the piperazinyl and carboxyl groups, with acid dissociation constants (pKa) values of 6.22 and 8.51, respectively [100]. The implication of this is that NRFX exists in its cationic state at pH less than 6.22 and in its anionic state at pH greater than 8.51. Therefore, for optimum sorption, an adsorbent with a negatively charged surface is required for the uptake of NRFX at low pH, and a positively charged adsorbent surface is required for NRFX uptake at high pH due to electrostatic attraction. According to Fang, Miao [85], in the pH range of 6.2–8.5, where NRFX exists in its zwitterionic state, hydrogen bonds and van der Waals forces, rather than electrostatic forces, would dominate its adherence to the active sites of the adsorbent.

Research conducted by Feng, Liu [3] obtained a declining trend in NRFX adsorption capacity with an increase in temperature from 20 °C to 40 °C using biochar derived from Luffa sponge. Similar observations were also made by Chen, Li [101] using iron-based mesoporous material (Fe-MCM-41) as an adsorbent. Niu, Liu [102] obtained an opposite result as increase in temperature from 25 °C to 45 °C, improved the adsorption capacity from 746 mg/g to 798 mg/g. Similar observations have also been obtained by several studies [103,104]. This disparity in Q_{max} value with respect to the change in temperature is hinged on the reaction temperature type. If the NRFX adsorption process is exothermic, decreasing the temperature of such a process is expected to increase the Q_{max} value [105]. A similar trend would also come into play by increasing the temperature of an endothermic reaction [106]. All things being equal, increasing the temperature of an exothermic adsorption reaction or decreasing the temperature of an endothermic adsorption reaction would lead to a decrease in Q_{max} . Other process parameters which can affect the adsorbent performance for NRFX uptake include adsorption duration, adsorbent dosage, NRFX concentration, ionic strength of the NRFX solution, and the presence of other chemical species in the solution matrix.

Adsorption mechanism

Understanding how well an adsorbent can remove a certain pollutant depends largely on the adsorption mechanism. This section discusses the adsorption mechanisms behind the interactions between NRFX and various adsorbents. Before focusing on particular adsorption mechanisms, it is important to analyze both empirical findings and analytical characterizations [143]. This is crucial since there are several processes involved in the adsorption of NRFX. The solution pH, the pH of the point of zero charge (pH_{pzc}), the adsorbate pKa, isotherm and kinetic studies, thermodynamic studies, and desorption studies are all important variables in establishing

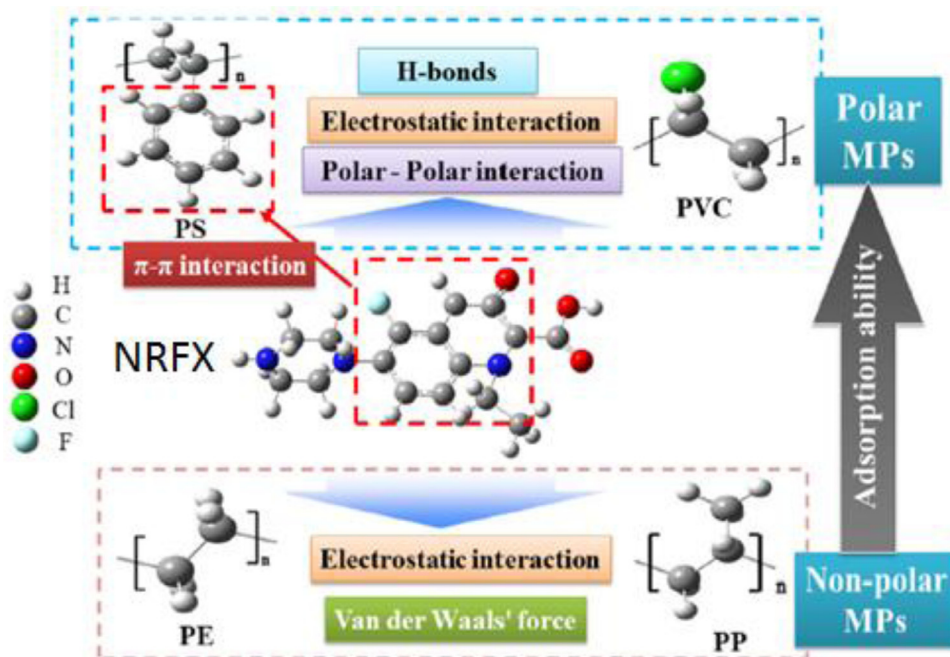


Fig. 2. Schematic representation of NRFX adsorption on different microplastics (PP, PVC, PE, and PS). Reprinted from Zhang, Ni [12] with permission from Elsevier.

the mechanism of adsorption. The pH_{pzc} is the pH of the solution when the amount of positive charges on the adsorbent surface equals the amount of negative charges. When the $\text{pH} < \text{pH}_{\text{pzc}}$, the adsorbent surface is protonated and positively charged, but when the $\text{pH} > \text{pH}_{\text{pzc}}$, the surface is deprotonated and negatively charged [144]. NRFX has two proton-binding sites (carboxyl and piperazinyl groups) with respective pK_a values of 6.22 and 8.51 [10]. When the pK_a is less than 6.22, NRFX exists as NRFX^+ (cationic form). It exists as NRFX^\pm (zwitterionic form) when the pK_a is between 6.22 and 8.51, and as NRFX^- (anionic form) when the pK_a is greater than 8.51 [104].

The mechanisms of NRFX adsorption onto various adsorbents are comprehensively summarized in Table 3, along with the optimum pH and pH_{pzc} . According to the table, the main adsorption mechanisms for NRFX uptake include electrostatic interactions, H-bonds, π - π interactions, electron donor-acceptor interactions, hydrophobic interactions, and pore diffusion. Van der Waals forces, cation exchange, and surface complexation are a few additional often observed interactions. An electron donor-acceptor (EDA) interaction is typically used to describe the adsorption mechanism of ionic organic molecules on carbonaceous sorbents [114]. π - π EDA interaction is a specific and non-covalent bond that widely exists between electron-rich and electron-poor compounds [91]. NRFX is a strong acceptor compound due to the presence of a fluorine group in its chemical structure, which has a high tendency to attract electrons [145,146]. Other π interactions reported include, π - π stacking interactions [80,147,148] and n - π interactions [128].

The protonation and deprotonation of NRFX pH_{pzc} can promote electrostatic interaction, which is the interaction of molecules with opposing charges, resulting in electrostatic attraction or repulsion between the adsorbent surface and the adsorbate [149]. H-bond and van der Waals forces are relatively weak interactions that arises as a result of intermolecular dipole-dipole forces [149,150]. Numerous moieties found in the NRFX molecules engage with the adsorbent's surface functional groups to create H-bonds [100]. Hydrophobic interactions are non-covalent forces in which nonpolar species have the tendency to cluster in solution [150]. The formation of hydrophobic interactions is facilitated by the zwitterionic form of NRFX [9]. Pore filling entails the adsorption of contaminants onto meso- and microporous adsorbents (like biochar) [151]. The various interactions operate at different pH of the solution. For example, in the adsorption of NRFX onto the surface of montmorillonite/wheat straw-derived biochar composite [100], electrostatic attraction between negatively charged NRFX and the biochar surface dominated the mechanism at $\text{pH} < 5$, while H-bond between NRFX molecules and oxygen-containing groups, as well as pore fillings, were the dominant mechanisms at $\text{pH} > 5$.

The adsorption mechanism can also be ascertained using analytical methods, such as FTIR, XPS, and XRD, as they reveal the functional groups present in the system and the positions of their interactions [152,153]. Zhang, Ni [12] used a combination of isotherm and kinetic studies, as well as various spectroscopic analyses, to determine the general adsorption mechanisms in the sorption of NRFX from simulated natural water and real surface water onto four different types of microplastics (polyethylene (PE), polystyrene (PS), polypropylene (PP), and polyvinyl chloride (PVC)) (Fig. 2). Several elements, such as H, C, N, O, Cl, and F, were detected on the microplastics using the XPS analysis, while FTIR revealed the presence of peaks assigned to hydroxyl and H-bonds. As depicted in Fig. 2, the microplastics can generally adsorb NRFX by a variety of mechanisms, including electrostatic, H-bond, van der Waals, π - π , and polar-polar interactions.

Table 3
Adsorption mechanisms for NRFX removal (NRFX pKa₁ = 6.22 and pKa₂ = 8.51).

Adsorbent	Optimum pH	pHpzc	Adsorption mechanism	Ref.
Montmorillonite-biochar	11	6.9	Electrostatic interactions, H-bonds, pore-filling	[100]
Urea N-doped biochar	5.0	4.0	H-bonds, pore-filling, π - π EDA	[135]
N-doped/activated cocoa shell biochar	5.0	4.1	Pore-filling, H-bonds, π - π EDA, ion exchange, electrostatic attractions	[98]
UIO-66-NH ₂ nanomaterials	8.0	–	Electrostatic interactions, π - π interactions, H-bonds	[9]
Ni-Al LDH	7.0	7.3	Electrostatic interactions, anion exchange, hydrophobic interactions	[34]
Silica	8.2	9.0	Electrostatic interactions	[154]
Ferrihydrite nanoparticles	5.5	–	Electrostatic interactions, complexation	[155]
Bentonite-sludge biochar composite	6.0	–	H-bonds, complexation, precipitation, Electrostatic interactions, π - π interactions	[8]
Pretreated barley straw	6.7	4.1	Electrostatic attractions, H-bonds, π - π interactions, π - π EDA	[111]
Polydopamine microspheres	7.0	6.3	H-bonds, electrostatic interactions, π - π interactions	[80]
Microplastics	5.0	–	π - π conjugation, H-bonds, ion exchange, electrostatic interactions	[7]
Dissolved organic matter	7.0	–	π - π interactions, electrostatic interactions, H-bonds, van der Waals forces	[4]
(Fe/Zn + H ₃ PO ₄)-modified sludge biochar	7.0	2.2	H-bonds, π - π interactions, electrostatic interactions, complexation	[133]
N rich- <i>Calotropis gigantean</i> fiber	8.0	–	Hydrophobic interactions, electrostatic interactions, H-bonds, π - π stacking interactions	[125]
Loofah AC	–	–	Physisorption, π - π interactions	[89]
Magnetic biochar from furfural residue	4.0	3.4	Electrostatic attractions, π - π EDA, van der Waals forces	[138]
Microplastics	5.0	4.5	Electrostatic interactions, π - π interactions, H-bonds, polar-polar interactions, van der Waals forces	[12]
Rice husk (<i>Oryza sativa</i>)	6.2	5.2	Electrostatic interactions, H-bonds	[16]
Coffee husk (<i>Coffea arabica</i>)	6.2	4.1	Electrostatic interactions, H-bonds	[16]
Montmorillonite	4.5	–	Complexation	[157]
Functionalized CNTs	–	–	π - π EDA, H-bonds	[145]
Iron ore waste	7.0	8.5	Cation exchange	[15]
Magnetic porous carbon-based sorbent	7.0	7.6	Electrostatic interactions, hydrophobic interactions, H-bonds, π - π EDA	[91]
Hematite/biochar composite	4.0	7.7	π - π EDA, H-bonds, ion exchange, complexation	[139]
Pyrite/biochar composite	10	4.0	π - π EDA, H-bonds, ion exchange, complexation	[139]
rGO/magnetic composites	6.2	–	π - π interactions, electrostatic repulsion	[134]
Potato stem/clay biochar composite	11	7.8	Electrostatic interactions, hydrophobic interactions, H-bonds, π - π EDA	[10]
Layered chalcogenide	4.0	–	Electrostatic attractions, π - π stacking interactions	[115]
Mg/Fe layered biometallic hydroxide	6.0	–	Coordination bonds, H-bonds	[127]
Activated magnetic biochar	7.0	–	π - π interactions, electrostatic force, pore fillings	[78]
Amine-functionalized magnetic bamoboo-based AC	6.0	8.2	π - π EDA, electrostatic interactions, hydrophobic interactions, H-bonds	[33]
KOH-modified biochar	7.0	–	Electrostatic interactions, π - π EDA, H-bonds	[158]
Chitosan/ γ -Fe ₂ O ₃ composites	7.0	–	H-bonds	[86]
Iron-doped activated alumina	6.5	6.5	Cation bridging, surface complexation	[110]
Lotus stalk-based AC	5.5	5.4	Hydrophobic interactions, cation exchange, π - π EDA	[110]
Carboxylated WMCNTs	5.4	3.5	Electrostatic interactions, H-bonds	[121]
Macroporous resin	5.4	–	Hydrophobic effect	[121]
Hypercrosslinked resin aminated polystyrene resin	5.4	4.8	Micropore fillings, electrostatic interactions, H-bonds, π - π EDA, hydrophobic effect	[121]
Fe-MCM-41	3.0	3.3	Hydrophobic effect, surface complexation, π - π interactions, electrostatic interactions	[101]
Pretreated barley straw	7.0	–	π - π EDA, H-bonds, electrostatic interactions, hydrophobic interactions	[90]
Pomelo peel-based biochar	3.0	11	Cation exchange, H-bonds	[104]
γ -Fe ₂ O ₃ /biochar	5.0	5.9	Cation exchange, H-bonds, hydrophobic interactions	[104]
H ₂ SO ₄ -treated termite feces	8.0	1.7	π - π interactions, H-bonds, electrostatic interactions	[5]
Fe/Cu oxides nanocomposites	7.0	3.7	Electrostatic interactions, surface complexation, H-bonds, π - π EDA	[103]
Shaddock peel-derived N-doped AC	7.0	8.0	π - π EDA, hydrophobic effect, H-bonds, electrostatic interactions, Lewis acid-base effect	[102]
Carbon/montmorillonite hybrid	7.0	2.0	H-bonds, electrostatic interactions, π - π EDA	[2]
MCM-41 mesoporous silica	7.0	–	π - π interactions, hydrophobic interactions	[130]
Graphene oxide	7.0	3.9	Van der Waals force, π - π interactions, hydrogen bond donor and acceptor	[17]
Fe/mesoporous silica	7.0	3.6	Electrostatic interactions, π - π EDA, H-bonds, surface complexation	[128]

(continued on next page)

Table 3 (continued)

Adsorbent	Optimum pH	pHpzc	Adsorption mechanism	Ref.
Cu/mesoporous silica	7.0	5.1	Electrostatic interactions, n- π EDA, H-bonds, surface complexation	[128]
Polydopamine microspheres	6.0	6.3	Electrostatic interactions, H-bonds, π-π stacking interactions	[80]
3D pretreated peanut shell/graphene oxide	6.2	-	Electrostatic interactions, H-bonds, π-π conjugation, hydrophobic effect	[118]
Pomelo peel-derived AC/phosphoric acid	7.0	6.3	Electrostatic H-bonds, hydrophobic interactions	[126]
Luffa sponge biochar	6.0	1.8	Cation exchange, electrostatic interactions	[3]
Temperature-switchable graphene oxide	7.0	-	π-π EDA, H-bonds	[159]
MOF/graphene oxide composite	7.0	-	Electrostatic interactions, π-π interactions, H-bonds	[83]
Carbon/montmorillonite hybrids	5.0	-	π-π EDA, electrostatic interactions	[116]
Magnetic biochar from salix mongolica	9.0	5.8	π-π dispersion, hydrophobic interactions, H-bonds, electrostatic interactions	[120]
Hydroxyapatite/polymeric nanocomposite	7.0	7.2	Physisorption	[6]
Iron-trimesic MOFs	7.0	3.6	Coordination bonds, pore filling, π-π stacking interactions	[112]
Cassava dreg biochar	7.0	-	H-bonds, π-π interactions	[160]
Fe/Cu oxides composite particles	8.1	4.0	h-bonds, π-π stacking interactions, surface complexation, hydrophobic interactions	[148]
Humic acid	3.0	-	Cation exchange	[161]
MgO/chitosan/graphene oxide	7.0	5.5	Electrostatic interactions, π-π EDA	[92]
MIL-101(Cr)-SO ₃ H	7.0	-	Electrostatic interactions	[99]
UiO-66-NH ₂ @TpTGcl	8.0	-	Electrostatic interactions	[117]
ZIF-8	6.0	-	Electrostatic interactions, π-π stacking interactions	[147]
Mg-Al-CO ₃ -LDH	8.7	8.7	Electrostatic attraction	[136]
Mg-Al-Cl-LDH	8.0	9.5	Electrostatic attraction, anion exchange	[136]

Isotherm and kinetic modeling

Isotherm studies

The knowledge of adsorption equilibrium is the most significant information required for effective interpretation of any adsorption process [34,181]. Analysis of adsorption is very essential for the general enhancement of process mechanism pathways and useful design of adsorption systems [159,133]. Adsorption isotherm study of any pollutant is carried out at constant temperature levels [182].

According to the information in Table 4 and Fig. 3(a), it is discernible that the adsorptive uptake of NRFX by various adsorbents were most suitably described by Langmuir isotherm (57%), followed by Freundlich isotherm (26%). This implies that NRFX adsorption is majorly monolayer in nature, where active sites exhibit uniform affinity for NRFX molecules [1,142]. However, NRFX uptake can involve multilayer adsorption occurring on heterogeneous surfaces, which form the main assumptions of Freundlich isotherm observed in 26% of the reviewed works (see Fig. 3 (b)). It is interesting to highlight that significant type of adsorbents involved in Freundlich's multilayer adsorption are thermal derivatives of biobased materials such as biochar [133,135,160], and activated carbon [113,126]. This could be attributed to the fact that biochar and activated carbon are characterized by irregular lamellar structure, which enhances its heterogeneous surface to promote multilayer adsorption of NRFX [3,114,141]. Aside Langmuir and Freundlich isotherm, a few other equilibrium models which effectively described NRFX adsorption include Redlich-Peterson [16,80,108,183], Sips [5,14,104], Dubinin-Astakhov [91,111], Koble-Corrigan [102,120], Polanyi-Manes [157], and Temkin [134].

Given that Langmuir and Freundlich isotherms were the dominant models that best described NRFX uptake, it is imperative to briefly elucidate these models and their associated parameters. The nonlinear form of Langmuir isotherm is given by Eq. (1).

$$q_e = \frac{K_L q_m C_e}{K_L C_e + 1} \tag{1}$$

Where C_e is equilibrium NRFX concentration (mg/L), q_e is equilibrium adsorption capacity (mg/g), K_L is the Langmuir constant (L/mg), q_m is the theoretical maximum monolayer coverage (mg/g). Linearising Eq. (1) will give Eq. (2).

$$\frac{C_e}{q_e} = \frac{1}{K_L q_m} + \frac{C_e}{q_m} \tag{2}$$

Plot of $\frac{C_e}{q_e}$ vs C_e will give $\frac{1}{q_m}$ and $\frac{1}{K_L q_m}$ as slope and intercept, respectively.

Freundlich has the nonlinear form given in Eq. (3).

$$q_e = K_f C_e^{1/n} \tag{3}$$

Where K_f represents the Freundlich constant, $1/n$ represents the heterogeneity factor. $1/n$ and K_f are obtained as slope and intercept from plotting $\text{Log } q_e$ vs $\text{Log } C_e$ of the linear form given in Eq. (4).

$$\text{Log } q_e = \text{Log } K_f + (1/n) \text{Log } C_e \tag{4}$$

Table 4
Isotherm and kinetic parameters.

Adsorbent	Isotherm			Kinetics			Ref.
	Best Fit	Nature	R ²	Best Fit	Nature	R ²	
Octahedral UiO-66-NH ₂ nanomaterials	Langmuir	Nonlinear	0.9930	PSO	Linear	0.999	[9]
Tailored N-doped biochar from corn stalk	Freundlich	Nonlinear	0.9780	Elovich	Nonlinear	0.999	[135]
Biochar corn stalk	Langmuir	Nonlinear	0.9950	–	–	–	[135]
CoFe ₂ O ₄ @TiO ₂ -MMIP	Langmuir	Nonlinear	0.9945	PSO	Nonlinear	0.9940	[15]
N-doped biochar derived from cocoa shell	Langmuir	Nonlinear	0.9990	Elovich	Nonlinear	0.9990	[98]
montmorillonite-biochar composite	Langmuir	Nonlinear	0.9950	–	–	–	[28]
animal hairs-based activated carbon	Freundlich	Nonlinear	0.9967	PSO	Nonlinear	0.9999	[113]
Polydopamine microspheres	Redlich-Peterson	Nonlinear	0.9990	PSO	Nonlinear	0.984	[80]
H ₃ PO ₄ pretreated Raw barley straw	Dubinin-Astakhov	Nonlinear	0.980	PSO	Linear	0.990	[111]
Bentonite enhanced sludge biochar composite	Sips	Nonlinear	0.9763	–	–	–	[8]
ferrihydrate nanoparticles	Langmuir	Nonlinear	0.9970	PSO	Nonlinear	0.978	[155]
Biochar derived from spent coffee ground	Langmuir	Nonlinear	0.9740	–	–	–	[129]
Ceramic membrane	Langmuir	Nonlinear	0.9750	PSO	Nonlinear	0.997	[35]
Imprinted polymer microsphere (PMS@MIPs)	Freundlich	Linear	0.9950	PSO	Linear	0.9999	[112]
Non-imprinted polymer microsphere (PMS@NIPs)	Freundlich	Linear	0.9960	PSO	Linear	0.9999	[119]
Loofah activated carbon	Langmuir	Nonlinear	0.981	PSO	Linear	0.9820	[72]
Monomer molecularly imprinted sol-gel polymers from magnetic halloysite nanotubes	Freundlich	Nonlinear	0.9904	PSO	Nonlinear	0.9987	[109]
Nitrogen-rich Calotropis gigantea fiber	Freundlich	Nonlinear	0.9891	PSO	–	0.9993	[125]
modified sludge biochar	Freundlich	Nonlinear	0.9970	Elovich	Nonlinear	0.9660	[133]
Microplastics	Langmuir	Nonlinear	0.9970	PSO	Linear	0.9990	[7]
modified meta kaolin	Langmuir	Linear	0.9790	PSO	Nonlinear	0.9960	[1]
iron ore waste	Langmuir	Nonlinear	0.9990	PSO	Nonlinear	0.9990	[15]
mesoporous silica	Langmuir	Nonlinear	0.9883	–	–	–	[15]
carbon nanotubes	Polanyi–Manes	Nonlinear	1.0000	–	–	–	[157]
rice (Oryza sativa) husk wastes	Redlich-Peterson	Nonlinear	0.9950	PSO	Nonlinear	1.0000	[16]
coffee (Coffea arabica) husk wastes	Redlich-Peterson	Nonlinear	0.9960	PSO	Nonlinear	1.0000	[16]
Microplastics	Langmuir	Nonlinear	0.9830	PSO	Nonlinear	0.9920	[12]
Magnetic biochar	Freundlich	Nonlinear	0.9970	PSO	Linear	0.982	[114]
bamboo-based magnetic activated carbon	Langmuir	Nonlinear	0.9990	–	–	–	[34]
Plant based biochar	Langmuir	Nonlinear	0.9982	PSO	Nonlinear	0.9731	[78]
Mg/Fe bimetallic hydroxide	Freundlich	Linear	0.9990	PSO	Nonlinear	0.9990	[127]
Chalcogenide	Langmuir	Linear	0.999	–	–	–	[138]
graphene oxide/magnetite composites	Temkin	Nonlinear	0.999	PSO	Nonlinear	0.9999	[134]
clay-biochar composite	Langmuir	Nonlinear	0.97	PSO	Linear	0.99	[10]
iron ore – biochar composites	Freundlich	Nonlinear	0.9913	PSO	Linear	0.9995	[139]
MOF-derived carbon-based sorbent	Dubinin-Astakhov	Nonlinear	0.948	–	–	–	[55]
MOF@iCOF composite	Langmuir	Linear	0.999	PSO	Linear	0.996	[117]
iron and nitrogen co-doped biochar	Langmuir	Linear	0.9986	PSO	Linear	0.9895	[184]
ZIF-8 metal-organic framework	Freundlich	Nonlinear	0.981	PSO	Nonlinear	0.999	[147]
pretreated barley straw	Langmuir-Freundlich	Nonlinear	0.955	PSO	Linear	0.999	[90]
Fe-MCM-41 molecular sieves	Freundlich	Nonlinear	0.9906	PSO	Nonlinear	0.9990	[101]
Mg–Al layered double hydroxides	Freundlich	Linear	0.9952	PSO	Nonlinear	0.9999	[136]
porous resins	Langmuir	Nonlinear	0.999	PSO	Nonlinear	0.99	[139]
carbon nanotube	Langmuir	Nonlinear	0.999	PSO	Nonlinear	0.99	[139]
lotus stalk-based activated carbon	Langmuir	Nonlinear	0.9996	PSO	Nonlinear	0.9990	[110]
iron-doped activated alumina	Freundlich	Nonlinear	0.9931	PSO	Nonlinear	0.9990	[110]
Chitosan	Langmuir	Nonlinear	0.997	PFO	Nonlinear	0.916	[36]
chitosan/Fe ₂ O ₃ composites	Langmuir	Nonlinear	0.993	PSO	Nonlinear	0.878	[36]
KOH modified biochar	Langmuir	NS	0.9300	PSO	–	0.9700	[158]
Pomelo Peel Activated Carbon	Freundlich	Nonlinear	0.9970	PSO	Nonlinear	0.9900	[126]
Carbon/montmorillonite	Langmuir	Nonlinear	0.99	–	–	–	[2]
mesoporous metallic silicon	Langmuir	Nonlinear	0.998	PSO	Linear	0.999	[128]
magnetic biochar	Koble-Corrigan	Nonlinear	0.999	Elovich	Nonlinear	0.990	[20]
luffa sponge biochar	Freundlich	Nonlinear	0.9995	PSO	NS	0.9998	[3]
Graphene Oxide	Langmuir	Nonlinear	0.996	PSO	Nonlinear	0.972	[159]
MOF@GO composite	Langmuir	Linear	0.99929	PSO	Linear	0.937	[83]
montmorillonite	Langmuir	Nonlinear	0.98	–	–	–	[116]
carbon/montmorillonite hybrids	Langmuir	Nonlinear	0.99	–	–	–	[116]
fly ash	Langmuir	Nonlinear	0.982	Elovich	Nonlinear	0.997	[122]
Acid-modified fly ash	Langmuir	Nonlinear	0.998	Elovich	Nonlinear	0.995	[122]
Alkali-modified fly ash	Langmuir	Nonlinear	0.955	PSO	Nonlinear	0.992	[122]
Molecularly imprinted polymer	Freundlich	Linear	0.9970	PSO	Linear	0.9829	[81]
magnetic molecularly imprinted polymers	Freundlich	Linear	0.976	PFO	Linear	0.9607	[132]
MOFs	Langmuir	Nonlinear	0.9994	PSO	NS	0.9999	[99]

(continued on next page)

Table 4 (continued)

Adsorbent	Isotherm			Kinetics			Ref.
	Best Fit	Nature	R ²	Best Fit	Nature	R ²	
Cassava Dreg Biochar	Freundlich	Linear	0.9980	PSO	Nonlinear	1.000	[160]
Fe/Cu oxides composite	Redlich-Peterson	Nonlinear	0.9980	Double-constant rate	Nonlinear	0.999	[108]
microporous activated carbon	Langmuir	Linear	0.9999	PSO	Linear	0.9975	[123]
iron-trimesic metal-organic frameworks (Fe-BTC)	Langmuir	Nonlinear	0.9950	PSO	Nonlinear	0.9990	[112]
Chitosan-based sorbent	Langmuir	Linear	0.997	PSO	Linear	0.9950	[92]
chitosan-hydroxyapatite	Langmuir	Nonlinear	0.99	PSO	Linear	0.99	[6]
hexagonal mesoporous silica	Langmuir	NS	0.9950	PSO	NS	–	[130]
copper-porphyrin MOF	Langmuir	Linear	0.9990	PSO	Linear	0.9990	[131]
Humic acid	Freundlich	Nonlinear	0.985	–	–	–	[161]
Nano Alumina	Langmuir	Linear	0.979	PFO	Linear	0.993	[13]
Carbonized Moringa pod husks	Freundlich	Linear	0.995	Blanchard	Linear	0.989	[141]
Ammonium chloride-treated	Langmuir	Linear	0.991	Blanchard	Linear	0.988	[141]
Amino-functionalized Zr-based MOF	Langmuir	Nonlinear	0.993	PFO	Linear	0.999	[9]
Graphene oxide	Sips	Nonlinear	0.997	PSO	–	–	[17]
KOH-modified biochar	Langmuir	Nonlinear	0.93	PSO	Linear	0.970	[158]
Polydopamine microspheres	Redlich-Peterson	Nonlinear	0.999	PSO	Nonlinear	0.984	[80]
peanut shell-supported graphene oxide (PPS/GO)	Freundlich	Nonlinear	0.9611	PSO	Linear	0.9999	[118]
BC	–	–	–	PSO	Nonlinear	0.980	[137]
BC	Sips	Nonlinear	0.9955	PSO	Nonlinear	0.9938	[54]
γ-Fe2O3@BC	Sips	Nonlinear	0.9986	PSO	Nonlinear	0.9742	[54]
Acid activated termite feces	Sips	Nonlinear	0.9976	PSO	Nonlinear	0.9941	[5]
Modified Activated Carbon	Langmuir	Nonlinear	0.9656	PSO	Nonlinear	0.9540	[146]
N-doped activated carbon	Koble-Corrigan	Nonlinear	0.9996	PSO	Nonlinear	0.9996	[102]
BC	Langmuir	NS	0.9939	PSO	Nonlinear	0.9978	[8]
Magnetic biochar-based Manganese oxide	Langmuir	NS	0.9694	PSO	Nonlinear	0.9999	[8]
Modified TiO ₂	Langmuir	Nonlinear	0.9990	PSO	Nonlinear	0.9980	[46]
Activated Carbon	Langmuir	Nonlinear	0.9937	PSO	Nonlinear	0.9993	[107]
Magnetic MIP	Langmuir	Nonlinear	0.9910	PSO	Linear	0.9960	[185]
Granular activated carbon	Freundlich	Nonlinear	0.9890	PSO	Nonlinear	1.0000	[124]
Activated carbon from agro waste	Redlich-Peterson	Nonlinear	0.9930	Elovich	Nonlinear	0.9980	[183]

Adsorption kinetics

Adsorption kinetics is traditionally illustrated by sorption vs. time plot [181]. This plot determines the initiation of all kinetic investigations because its shape and outlook indicates the fundamental kinetics of any process [146,8]. Furthermore, sorption kinetics provide prerequisite reaction parameters and facilitates in estimating thermodynamic data required for design and ultimate scale-up of lab-model experiments [112]. From the data collected for kinetics in Table 4 and the associated pie chart in Fig. 3(b), it is apparent that the adsorption of NRFX is best described by pseudo-second order (PSO) model, while a few works (16%) reported the superiority of other models [36,98,133,135,13,132,141,183].

Pseudo-second order (PSO) model assumes a second order sorption rate with regards to available active sites [181]. The linear and nonlinear forms of PSO are given in Eqs. (5) and (6), respectively.

$$q_t = \frac{k q_e^2 t}{1 + k q_e t} \tag{5}$$

$$\frac{t}{q_t} = \frac{1}{k q_e^2} + \frac{t}{q_e} \tag{6}$$

Where k is the kinetic rate constant, and q_t is the adsorption capacity at time, t. A plot of $\frac{t}{q_t}$ vs. t produces a straight line for PSO conforming kinetics [9,111,119].

The acceptability of PSO equation in accurate modeling of adsorption processes has been challenged by two major drawbacks: the first is over-fitting anomalies associated with the model [182], the other is unreliable prediction of the linear form of PSO owing to regression errors [188]. However, the work of Tran et al. [182] demonstrated that PSO model, regardless of the form, performed satisfactorily better than other models in adsorption kinetics of antibiotics similar to NRFX. In view of the fact that PSO was superior in the prediction of NRFX adsorption kinetics, it follows that the fundamental assumptions of the model such as a chemisorption process which features adsorbate-to-adsorbent electron transfer, dominates the chelation process [181].

Thermodynamic studies

Thermodynamic studies provide data relating to temperature changes in a process. This information is exemplified by the values of thermodynamic parameters such as Gibbs free energy (ΔG°), change in enthalpy (ΔH°), and entropy (ΔS°) [186]. These parameters

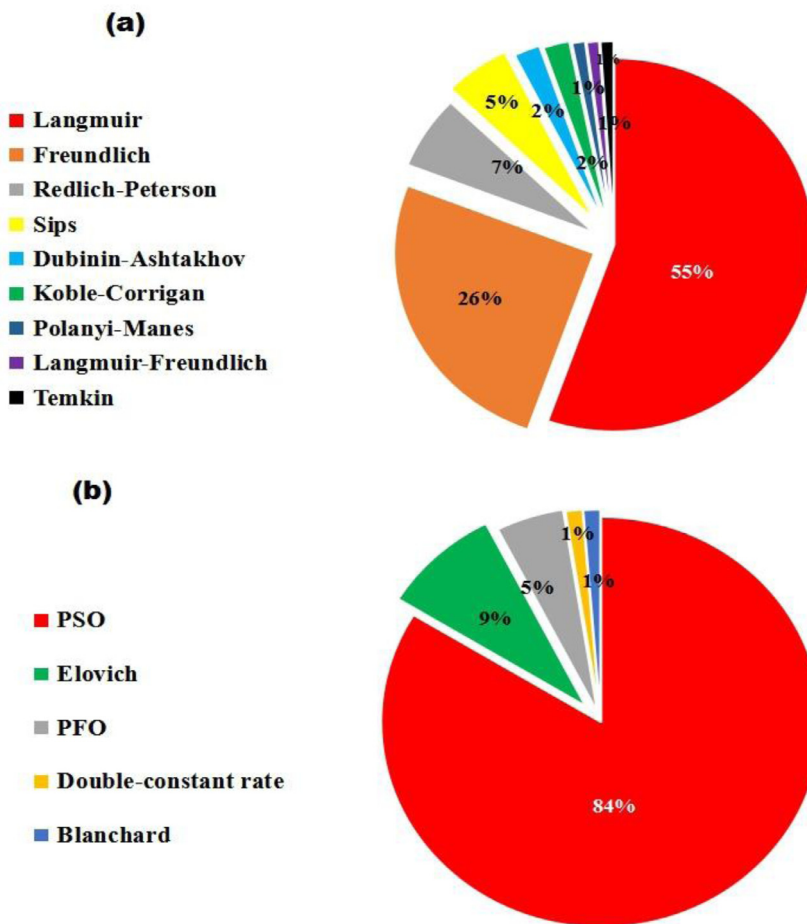


Fig. 3. Isotherm and kinetic adsorptive uptake of NFRX by various adsorbents distribution.

portray the favor-ability, spontaneity, energy delivery (exothermic) or utilization (endothermic), and degree of randomness of any process under investigation [8]. The thermodynamic parameters are estimated from Van't Hoff model, and the free energy equation given in Eqs. (7) and (8), respectively.

$$\ln K = \frac{\Delta S}{R} - \frac{\Delta H}{RT} \tag{7}$$

$$\Delta G = (\Delta H - T) \Delta S \tag{8}$$

Where K is the equilibrium constant, R is the universal gas constant and T is the temperature of the system in kelvin. The thermodynamic studies summarized in Table 5 reveals that NFRX adsorption onto biochars [78,103], activated carbon [123,141], clay-biochar composite [10,8], metal organic frameworks [83,147], modified biosorbents [157], and polymers [7,80], were majorly favorable as illustrated by decrease in ΔG° values occasioned by temperature increment. Furthermore, the negative ΔG° observed here indicates that NFRX uptake using these adsorbents was spontaneous at all temperature levels. This spontaneous and favorable outlook could be as a result of multi adsorption sites provided by oxygen loaded functional groups suitable for NFRX uptake [78,103]. A significantly different trend was observed for ferrous sorbents [54,139], where NFRX uptake was highlighted to be unfavorable even though the process maybe spontaneous. This implies NFRX uptake by magnetic adsorbents would be triggered by an external influence [54,186]. Non-spontaneity was observed by the use of synthetic polymers (PS, PBS, PE) indicating that NFRX adsorption requires energy to promote the process [7,80].

Enthalpy calculations specifies the nature and type of the adsorption process. Among all the adsorbents listed in Table 5 metallic compounds mainly exhibited exothermic ($H^\circ < 0$) nature, unlike other sorbants [8,101,169] where endothermic ($H^\circ > 0$) nature dominated the norfloxacin adsorption process. One probable justification for this endothermicity in terms of adsorption enthalpy is the inevitable loss of hydration layer from NFRX molecule at the point of adsorption [103,158]. This dehydration phenomenon utilizes more energy than exothermicity of NFRX molecules attached to the surface [158]. Similarly, NFRX uptake was observed to be predominantly physical type, with very few reports indicating chemisorption [160]. According to Chen et al., [187], the heat given off

Table 5
Thermodynamic parameters.

Adsorbent	Thermodynamic parameters				Ref.
	Temp (K)	ΔG° (kJ/mol)	ΔH° (kJ/mol)	ΔS° ($\text{J/mol}\cdot\text{K}$)	
CoFe ₂ O ₄ @TiO ₂ -MMIP	323	-2.28	11.35	40	[85]
Bentonite enhanced sludge biochar composite	313	- 9.33	6.03	49.06	[8]
Loofah activated carbon	298	- 5.97	-	-	[72]
modified sludge biochar	308	-7.23	3.84	0.0359	[133]
Potential of polystyrene (PS)	288	9.005	10.341	4.8	[7]
Polybutylene succinate (PBS)	298	9.945	3.541	-21.3	[7]
Polyethylene (PE)	288	12.799	30.312	62.0	[7]
iron ore waste	308.15	-33.01	-1.09	103.59	[15]
rice (<i>Oryza sativa</i>) husk wastes	338	-48.07	41.55	263.50	[16]
coffee (<i>Coffea arabica</i>) husk wastes	338	-45.33	4.858	148.40	[16]
Plant based biochar	308.15	- 4.5909	32.194	0.1196	[78]
Mg/Fe bimetallic hydroxide	298	- 5.5400	-41.41	0.12	[127]
graphene oxide/magnetite composites	308	-20.49	-19.17	4.30	[134]
clay-biochar composite	308.15	-1.924	22.50	0.079	[10]
Biochar	288.15	2.886	28.94	0.091	[10]
pyrite-biochar composites	288.15	-20.5437	-31.9914	-39.6	[139]
hematite-biochar composites	308.15	-17.2404	49.2746	216.8	[139]
ZIF-8 metal-organic framework	313	-6.27	5.68	39.00	[147]
Fe-MCM-41 molecular sieves	308	-5.09	13.92	61.73	[101]
Mg-Al layered double hydroxides (CO ₃ -MA21)	318	-17.61	-3.03	45.87	[136]
Mg-Al layered double hydroxides (Cl-MA21)	318	-20.50	-27.65	-22.21	[136]
KOH modified biochar	308	-15.54	6.13	70	[158]
mesoporous metallic silicon (Cu/SBA-15)	308	-2.60	10.28	41.82	[128]
mesoporous metallic silicon (Fe/SBA-15)	288	-2.39	-7.27	-16.96	[128]
magnetic biochar	308	-3.79	38.41	136.94	[20]
luffa sponge biochar	308	-30.55	-8.6	-126	[159]
MOF@GO composite	310	-13,324.33	-0.000011	-306.735	[83]
fly ash	288	-20.857	-35.541	-51	[122]
Acid-modified fly ash	288	-20.594	-27.372	-24	[122]
Alkali-modified fly ash	288	-21.573	-30.804	-32	[122]
Cassava Dreg Biochar	308	-78.60	326.40	1320	[160]
Fe/Cu oxides composite	313	-4.46	1.47	18.94	[108]
microporous activated carbon	303	-12.604	-30.362	-58.53	[123]
iron-trimesic metal-organic frameworks (Fe-BTC)	318	-12.935	5.903	59.24	[112]
Carbonize Moringa pod husks	328	-32.091	-23.919	24.443	[141]
Ammonium chloride-treated	328	-31.377	-13.203	5.662	[141]
Amino-functionalized Zr-based MOF	318	-8.76	8.401	54.014	[9]
Graphene oxide	304.15	-7.784	-13.141	-18	[17]
KOH-modified biochar	308	-21.06	31.26	17.00	[158]
Polydopamine microspheres	318	-17.4	7.30	77.6	[80]
BC	318.15	-1.9386	-10.5651	39.3865	[104]
γ -Fe ₂ O ₃ @BC	318.15	2.5136	6.9232	29.5070	[104]
Fe/Cu oxides composite	313	-4.32	2.72	22.5	[120]
Acid activated termite feces	328	-3.54	62.62	198.7	[5]
N-doped activated carbon	318	-37.83	34.73	230	[102]
BC	308	- 18.54	16.97	115.3	[8]
Magnetic BC/MnO ₂ composite	308	- 24.61	18.12	138.9	[8]

during physisorption process is identical in scale as the heat of condensation (Heat = 2.1 - 20.9 kJ/mol; Energy = -20 to 0 kJ/mol), while chemisorption energy and heat demands are found within the range of -80 to -400 kJ/mol and 80 - 200 kJ/mol, respectively. Given that physical adsorption dominates, it implies that the driving force is electrostatic (Van der Waals' force) interaction, where NRFX molecules are not restricted to a specific location on the adsorbent surface [7,8].

Entropy changes (ΔS°) signifies the degree of disorderliness (randomness) and also depicts the capacity of any adsorbent to remove the targeted adsorbate [186]. The entropy sign convention gives a hint of either increased randomness ($\Delta S^\circ > 0$) or reduced randomness ($\Delta S^\circ < 0$) of an adsorption process. From the change in entropy values outlined in Table 5, most adsorbents displayed strong affinity for NRFX adsorbate as illustrated by the positive entropy values. This phenomenon is attributed to the formation of well structured active sites following special functionalization procedures which aided efficient sequestration of NRFX on the surface of the adsorbent [112,160]. A few reports of reduced randomness were indicated by application of biochar [3,91], activated carbon [123], ferric sorbents [139], MOF [83], metallic compounds [59], and synthetic polymer [7]. This reduced randomness results from NRFX adsorption difficulties, which implies that the adsorbate molecules even after the adsorption process may likely remain in the bulk effluent. This drawback could be eliminated either by improving the adsorbent preparation step to produce better structured adsorbents, or ensuring that no other effluent is competing with the adsorbate of interest for occupation of active sites.

Table 6
Summary of competitive adsorption NRFX.

Adsorbent	Competing species	Maximum change with competing species	Ref.
Nanocomposite optosensor	Ciprofloxacin	No change	[165]
Magnetic molecularly imprinted polymer	K ⁺ , Na ⁺	Little influence	[85]
Magnetic molecularly imprinted polymer	Cu ²⁺	41.5% reduction	[85]
Magnetic molecularly imprinted polymer	Fe ²⁺	84.3%reduction	[85]
Magnetic molecularly imprinted polymer	Mn ⁺ , Al ³⁺ , Ca ²⁺ , Mg ²⁺	Decrease	[85]
N-doped/activated cocoa shell biochar	Na ⁺ , Ca ²⁺	Decrease	[98]
UIO-66-NH ₂ nanomaterials	NaCl, CaCl ₂	Increase	[9]
Spent coffee ground-derived biochar	Na ⁺ , Ca ²⁺	Decrease	[129]
Bentonite/sludge biochar composite	Na ⁺	Increase	[8]
Polydopamine microspheres	CaCl ₂ , NaCl	Decrease	[80]
Polystyrene microplastic	NaCl	76.8% decrease	[7]
Polybutylene succinate microplastic	NaCl	84.7% decrease	[7]
Polyethylene microplastic	NaCl	90.9% decrease	[7]
Dissolved organic matter	Na ⁺	Decrease	[4]
Surface molecularly imprinted polymer	Enrofloxacin, ciprofloxacin, sulfonamide	Increase	[119]
Magnetic biochar from furfural residue	Chloramphenicol, ciprofloxacin, tetracycline	Decrease	[114]
Microplastics	Humic acid	75.3% decrease	[12]
Iron ore waste	Na ⁺	25.4% decrease	[15]
Iron ore waste	Ca ⁺	45.3% decrease	[15]
Iron ore waste	Mg ²⁺	61% decrease	[15]
Hematite/biochar composite	Ca ²⁺	Increased at low concentration of Ca ²⁺ but decreased at high concentration	[139]
Pyrite/biochar composite	Ca ²⁺	Negligible effect	[139]
Amine-functionalized magnetic bamboo-based AC	NaCl	Slight increase	[34]
Fe-MCM-41	Na ⁺ , Ca ²⁺	Decrease	[155]
Pomelo peel-based biochar	Na ⁺	Decrease	[104]
γ-Fe ₂ O ₃ /biochar	Na ⁺	Increase	[104]
Fe/Cu oxides nanocomposites	NaCl, CaCl ₂	Decrease	[103]
Magnetic biochar-based/manganese oxide composite	CaCl ₂	Slight decrease	[138]
Zinc oxide/zinc sulfide composite	Fe ²⁺	10% increase	[20]
Zinc oxide/zinc sulfide composite	Na ⁺ , Cu ²⁺ , Zn ²⁺	Na ⁺ = Slight (2%) decrease, Cu ²⁺ = 99% decrease, Zn ²⁺ = 62% decrease	[20]
Zinc oxide/zinc sulfide composite	CO ₃ ²⁻	Slight increase	[20]
Zinc oxide/zinc sulfide composite	SO ₄ ²⁻ , NO ₃ ⁻ , Cl ⁻ , C ₆ H ₅ O ₇ ³⁻	Decrease	[20]
Polydopamine microspheres	NaCl, CaCl ₂	Decrease	[80]
3D pretreated peanut shell/graphene oxide	CaCl ₂	56% decrease	[118]
3D pretreated peanut shell/graphene oxide	NaCl	16.4% decrease	[118]
Pomelo peel-derived AC/phosphoric acid	Na ⁺	Slight decrease	[126]
Pomelo peel-derived AC/phosphoric acid	Mg ²⁺ , NO ⁻ , SO ₄ ²⁺	Sharp decrease	[126]
Temperature-switchable graphene oxide	Humic acid	Increase	[159]
Magnetic biochar from salix mongolica	NaCl, CaCl ₂	Decrease	[120]
Fe/Cu oxides composite particles	CaCl ₂	33% decrease	[148]
Fe/Cu oxides composite particles	NaCl	9% decrease	[148]

Generally, from analysis of results obtained from temperature effects, it is evident that NRFX adsorption is a physisorption process that is significantly spontaneous with increased surface randomness characterized by either exothermic (for non-metallic adsorbents) or endothermic nature (for metallic adsorbents).

Competitive adsorption

Since most wastewater contains some salts, the presence of these salts or co-ions in the solution may have an effect on the adsorption process. A competitive adsorption study is used to determine the ability of an adsorbent to selectively adsorb an adsorbate in the presence of other species vying for the available active sites on the surface of the adsorbent [162,163]. Determining the suitability of an adsorbent for practical wastewater treatment requires such a study [164].

The results of various experiments investigating the affinity of various adsorbents towards NRFX and other contaminants are shown in Table 6. In most of the studies, it can be seen that the presence of these other species led to a reduction in the absorption of NRFX. But some of them increased the removal impact [9,104,159], while others had no effect [139,165]. In the adsorption of NRFX using pomelo peel-based biochar and γ-Fe₂O₃-loaded biochar (γ-Fe₂O₃/BC) [104], it was discovered that the presence of Na⁺ reduced the adsorption of NRFX by the biochar adsorbent, and the reduction was stronger as the concentration of the Na⁺ increases (from 0.02 to 0.10 mol/L). This is due to the fact that Na⁺ may engage in cation exchange and rival NRFX for active binding sites on the biochar surface. A weaker H-bond will result between the biochar surface and NRFX as a result of the additional Na⁺ partially replacing the protons of the biochar surface. In contrast, adding Na⁺ increased the adsorption of NRFX by γ-Fe₂O₃/BC. This is because the ionic form of NRFX in water will be reduced by the additional NaCl, a process known as “salt-out-effect”, and will precipitate

Table 7
Summary of column adsorption for NRFX adsorption from aqueous media.

Adsorbent	Best-fit model	Conditions			Adsorption Capacity (mg/g)	Rate constant (1/min.mg)	Refs.
		Bed height (cm)	Vol. flow rate (mL/min)	Inlet Conc. (mg/L)			
<i>Phoenix dactylifera</i> L. based activated carbon	Thomas and Yoon-Nelson	25	0.5	150	1.992	46.2×10^{-5}	[169]
Amine-functionalized magnetic bamboo-based AC	–	60	0.5	300	315.7	–	[33]
Magnetic bamboo-based AC	–	60	0.5	300	193.4	–	[33]
Granular AC	–	25	1.5	225	–	–	[170]

into the molecular form of NRFX. The γ -Fe₂O₃/BC is then coupled with the NRFX of the molecular state via hydrophobic action to increase its adsorption capacity.

Liu, He [20] investigated the effect of competing ions for NRFX binding on the surface of a carbon-based composite photocatalytic material of zinc oxide and zinc sulfide (ZnO/ZnS@BC) using several cations (SO₄²⁺, NO₃⁻, Cl⁻, CO₃²⁻, C₆H₅O₇³⁻). The result revealed that NRFX degraded at varying rates in different ion solutions. For the cations, Fe²⁺ slightly enhanced the removal effect, while Na⁺ had almost no effect (only decreased by 2%). However, the removal effectiveness was significantly inhibited by Cu²⁺ and Zn²⁺ to the extent of 99% and 62%, respectively. This is due to the fact that NRFX caused the formation of new, structurally stable, and difficult-to-decompose clathrate in the presence of the cations. On the other hand, all the anions (with the exception of CO₃²⁻) hindered the removal effect, with NO₃⁻ showing the highest rate of inhibition (34%). CO₃²⁻ slightly promoted the removal of NRFX by ameliorating the pH of the solution [20].

Column adsorption

The adsorption of NRFX can be carried out in either a batch or continuous system. The latter is usually carried out with the aid of a fixed bed column [166,167]. Fixed-bed adsorption is more advantageous than batch adsorption as it is more effective and efficient in treating large quantities of polluted solutions, thus making the transition from laboratory to industrial treatment easier [168]. The pH of the environment, the height of the adsorbent bed, the NRFX flow rate in the column, the concentration of NRFX in the solution, the adsorbent quantity, and the number of regeneration cycles of the adsorbent bed all influence NRFX adsorption in a column. The summary of studies done by various authors for fixed bed adsorption of NRFX and the results obtained is given in Table 7.

Darweesh and Ahmed [169] studied the uptake of NRFX onto granular activated carbon (GAC) in a continuous packed bed column by varying the process parameters in a bid to obtain the optimum conditions for NRFX uptake. The volumetric flow rate was adjusted from 0.5 to 1.5 mL/min, the bed height was adjusted from 15 to 25 cm, and the initial concentration was adjusted from 75 to 250 mg/L. Results showed that the higher the flow rate, the lesser the interaction between GAC and NRFX, which would lead to a lower uptake capacity. The increase in bed height translates to more contact and diffusion time between NRFX and the pores of GAC. An increase in inlet concentration was noted to affect the uptake capacity the most in relation with other process variables, as an increase in NRFX concentration decreases the contact time between NRFX and GAC and also ensures improved filling of the adsorption site of the activated carbon [169]. The potential of using amine-functionalized magnetic bamboo-based activated carbon and non-functionalized magnetic bamboo-based activated carbon as adsorbents for NRFX uptake under similar conditions was explored by Peng, Hu [34]. The study revealed that since NRFX is a π -electron donor, the presence of the amine functional group, which is a π -electron acceptor on the surface of the adsorbent, contributed to the higher adsorption of the functionalized adsorbent [34].

Desorption and regeneration

A desorption/reusability study is usually carried out to determine how many times an adsorbent can be recycled and reused before its efficacy is jeopardized [143,171]. An adsorbent can be recovered by using an eluent to remove the NRFX from its surface. The percentage difference between the regenerated adsorbents' and the initial adsorbent's adsorption capacity is known as the adsorbent recovery [172,173]. This is especially significant because it reduces the cost of the process. Adsorption is typically more cost-effective if the adsorbent can be collected and recycled. The summary of several studies on the desorption and reusability of different adsorbents used for the adsorption of NRFX is shown in Table 8. It was observed that after 5 cycles, most of the adsorbents still had the ability to adsorb more than 75% of the initial concentration of NRFX. This shows the high recyclability of such adsorbents. The highest recovery of 97.10% after four regeneration cycles was obtained by Qin, Zhao [140] with the use of molecularly imprinted silica polymer and methanol/ethanol mixture as the eluent. For this to occur, different solvents have been utilized as eluents, with methanol and ethanol being the most commonly used. Yi, Liang [125] studied the desorption potential of nitrogen-rich *Calotropis gigantean* fiber using four different eluents. The eluents and their percentage desorption include aqueous sodium hydroxide (83%), hydrochloric acid (55%), sodium chloride (17%), and methanol (5%). This shows the efficiency of sodium hydroxide for the recyclability of NRFX-saturated adsorbents. The efficacy of sodium hydroxide as an eluent was also made in a study that reviewed that desorption/reusability of another antibiotics – levofloxacin [143]. In another study, Khan, Shaheen [83] observed that after three cycles of regeneration, graphene oxide/MOF based composite adsorbent gave a removal efficiency of 88.41%.

Table 8

Desorption and reusability of various adsorbents for NRFX adsorption from aqueous media.

Adsorbent	Elution agent	% qm after 1st cycle	Number of cycles (n)	% qm retained after n cycles	Refs.
Magnetic halloysite nanotubes/molecularly imprinted polymer composite	–	90.30	7	85.60	[109]
Molecularly imprinted polymer	HCOOH/CH ₃ OH (1:1)	90.00	6	> 85.00	[81]
Amino-functionalized Zr-based MOF	0.1 mol/L NaOH	> 95.00	5	> 80.00	[9]
Nitrogen-rich <i>Calotropis gigantean</i> fiber	0.1 mol/L NaOH	–	5	> 75.00	[125]
3D peanut shell/graphene oxide	C ₂ H ₅ OH _(aq)	89.73*	5	77.52*	[118]
Natural attapulgite-potato stem hybrid biochar	CH ₃ OH	84.20	5	82.00	[10]
Sawdust biochar/Al ₂ (SO ₄) ₃ -modified thermal kaolin	CH ₃ OH/H ₂ O	–	5	80.20	[1]
Amine-functionalized magnetic bamboo-based AC	C ₂ H ₅ OH _(aq)	–	5	80.00	[34]
Molecularly imprinted silica polymer	CH ₃ OH/ CH ₃ COOH (9:1 v/v)	–	4	97.10	[140]
Magnesium oxide/Chitosan/Graphene oxide	CH ₃ OH	–	4	> 80.00	[92]
Surface-imprinted polymer microsphere	CH ₃ OH/ CH ₃ COOH	83.20*	4	77.48*	[119]
Magnetic molecularly imprinted polymer composite	CH ₃ OH/ CH ₃ COOH	90.00	4	75.50	[132]
Graphene oxide/MOF based composite	C ₂ H ₅ OH/HCl (10:1)	93.61	3	88.40	[83]
Layered chalcogenide	1.0 M KCl	95.00	3	> 90.00	[115]
Magnetic potato stems and leaves biochar-based manganese oxide composite	–	98.00	3	95.00	[138]

* = mg/g.

Computer simulation of NRFX removal

Many approaches for molecular modeling of adsorption processes have been developed, including the force field method, quantum chemistry method, Monte Carlo method, and molecular dynamics method [174]. Molecular simulation employs a computer to construct molecular modeling at the atom level, which can then simulate the physical, chemical, and biological properties of molecular systems. Several studies have investigated various aspects of NRFX adsorption from aqueous solutions using a range of molecular modeling methodologies and computational tools. Li and Fang [174] utilised a computational chemistry tool called Hyperchem 8.0 for simulating molecule conformation and binding, and molecular mechanics optimiser was used to find the best molecular conformation. The total energies of the molecules were estimated after simulating the molecular conformations of the molecular imprinted particles (MIPs) with NRFX. The binding dynamics of NRFX to MIPs were investigated using molecular modeling and confirmed by binding studies. The energy changes of the molecules throughout the MIPs' binding process with NOR were computed, and the results were utilised to forecast the binding efficiency towards these molecules. There were two types of NRFX binding sites discovered on the molecular imprinted particles (MIPs). The first included hydrogen bonds between the oxygen atoms of MIPs and the carbonyl group of NRFX, while the second involved hydrogen bonds between the oxygen atoms of MIPs and the hydroxyl group of NRFX. Furthermore, the molecules' energies change was 1.69×10^6 J/mol. The results showed that the MIPs had good NRFX selectivity.

Dan, Li [118] investigated the adsorption of NRFX onto a 3D peanut shell/graphene oxide aerogel using DFT. Various interactions were involved in the adsorption of NRFX by 3D PPS/GO aerogel, including electrostatic attraction, H-bonding, π - π conjugation, and hydrophobic effect. Zhang, Cheng [175] used DFT calculations to determine the adsorption mechanism between sesame straw biochar ($935 \text{ m}^2\text{g}^{-1}$) and NRFX; computational simulations revealed that interactions between the biochar and NRFX were electrostatic interaction, hydrogen bond, and π - π interaction, all of which were conducive to chemical adsorption. The energy of adsorption for NRFX with biochar in water was 0.3977 Hartree. The higher the energy of adsorption, the more stable the adsorption arrangement between adsorbate and adsorbent. Yadav, Goel [176] also performed DFT calculations to determine the thermodynamic feasibility of the adsorption process and the nature of interactions of NRFX with the graphene oxide; the negative values of adsorption energy suggest the process's thermodynamic feasibility.

Additionally, computational investigations for NRFX uptake onto graphene oxides [177], graphene oxide/chitosan composites [178], and NRFX molecularly imprinted polymers [179] have been described.

Knowledge gaps and visions for the future

On the basis of this study of the literature, various knowledge gaps are highlighted below. Despite the recent publication of a great quantity of material on the absorption of NRFX via adsorption, numerous unresolved issues still exist and warrant further study. It is not possible to scale up a process for industrial use without investigations on column studies. Because fixed-bed adsorption is more effective and efficient at handling large amounts of contaminated solutions, it is preferable to batch adsorption. For column studies, just three researches were observed. Rarely is the waste management research on utilized adsorbents that will be discharged back into the environment highlighted in literature. It is advised that researchers consider alternatives to the usual combustion method for disposing of these adsorbents. Numerous academics have also noted a similar dearth of disposal studies [38,39,180]. For financial considerations and potential future applications of the described adsorbents, the budget of NRFX removal from pharmaceutical/hospital effluents is crucial.

Conclusion

This review's objective is to evaluate empirical data on NRFX's removal from aqueous medium. The environmental danger of IBP in the aquatic environment was validated by an initial ecotoxicological study. It is on the premise of the wide availability of research on NRFX adsorption that this review was conceived. Composite based adsorbents gave the highest NRFX adsorption capacities (Q_{max}) value for NRFX uptake, with Graphene oxide/ MOF giving 1114.8 mg/g. The type of adsorbent and the reactivity of the solution affect the adsorption process. The main adsorption mechanisms for NRFX uptake include electrostatic interactions, H-bonds, π - π interactions, electron donor-acceptor interactions, hydrophobic interactions, and pore diffusion. Langmuir isotherm and pseudo-second order kinetics models were superior in the prediction of NRFX which features adsorbate-to-adsorbent electron transfer on monolayer surface. The thermodynamics of NRFX adsorption is heavily dependent on the makeup of the adsorbent, and the selection of the eluent for desorption from the solid phase is equally important. The paper also examined several computational techniques that have been used by other studies to remove NRFX. There were detected knowledge gaps in adsorbent disposal and column investigations. Every research project will eventually be scaled up for commercial environmental protection applications.

Ethics statements

Not applicable.

Declaration of Competing Interest

The authors declare that they have no known competing financial interests or personal relationships that could have appeared to influence the work reported in this paper.

CRediT authorship contribution statement

Paschal Enyinnaya Ohale: Conceptualization, Writing – original draft, Writing – review & editing, Validation, Visualization. **Chinenye Adaobi Igwegbe:** Conceptualization, Supervision, Data curation, Writing – original draft, Writing – review & editing, Visualization. **Kingsley O. Iwuozor:** Writing – original draft, Writing – review & editing, Validation, Visualization. **Ebuka Chizitere Emenike:** Writing – original draft, Writing – review & editing, Validation, Visualization. **Christopher Chiedozie Obi:** Writing – original draft, Writing – review & editing, Validation, Visualization. **Andrzej Białowiec:** Supervision, Writing – review & editing, Validation, Visualization.

Data Availability

No data was used for the research described in the article.

Acknowledgments

This research did not receive any specific grant from funding agencies in the public, commercial, or not-for-profit sectors.

References

- [1] Y. Yang, et al., Efficient with low-cost removal and adsorption mechanisms of norfloxacin, ciprofloxacin and ofloxacin on modified thermal kaolin: experimental and theoretical studies, *J. Hazard. Mater.* 430 (2022) 128500.
- [2] M.E. Zelaya Soulé, et al., Carbon/montmorillonite hybrids with different activation methods: adsorption of norfloxacin, *Adsorption* 25 (7) (2019) 1361–1373.
- [3] Y. Feng, et al., Norfloxacin removal from aqueous solution using biochar derived from luffa sponge, *J. Water Supply: Res. Technol.-AQUA* 67 (8) (2018) 703–714.
- [4] Y. Wang, et al., Effects of dissolved organic matter on the adsorption of norfloxacin on a sandy soil (fraction) from the Yellow River of Northern China, *Sci. Total Environ.* 848 (2022) 157495.
- [5] T. Chahm, et al., Use of chemically activated termite feces a low-cost adsorbent for the adsorption of norfloxacin from aqueous solution, *Water Sci. Technol.* 79 (2) (2019) 291–301.
- [6] A. Nayak, B. Bhushan, S. Kotnala, Fabrication of chitosan-hydroxyapatite nano-adsorbent for removal of norfloxacin from water: isotherm and kinetic studies, *Mater. Today: Proc.* 61 (2022) 143–149.
- [7] M. Sun, et al., Adsorption behaviors and mechanisms of antibiotic norfloxacin on degradable and nondegradable microplastics, *Sci. Total Environ.* 807 (2022) 151042.
- [8] X. Cao, et al., Co-adsorption capabilities and mechanisms of bentonite enhanced sludge biochar for de-risking norfloxacin and Cu²⁺ contaminated water, *Chemosphere* 299 (2022) 134414.
- [9] X. Fang, et al., High-efficiency adsorption of norfloxacin using octahedral UiO-66-NH₂ nanomaterials: dynamics, thermodynamics, and mechanisms, *Appl. Surf. Sci.* 518 (2020) 146226.
- [10] Y. Li, et al., Removal of Norfloxacin from aqueous solution by clay-biochar composite prepared from potato stem and natural attapulgite, *Colloids Surf. A* 514 (2017) 126–136.
- [11] M. Feng, et al., Metal-mediated oxidation of fluoroquinolone antibiotics in water: a review on kinetics, transformation products, and toxicity assessment, *J. Hazard. Mater.* 344 (2018) 1136–1154.
- [12] Zhang, Y., et al., Mechanistic insight into different adsorption of norfloxacin on microplastics in simulated natural water and real surface water. *Environ. Pollut.*, 2021. 284: p. 117537.
- [13] A. Parashar, S. Sikarwar, R. Jain, Studies on adsorption kinetics of norfloxacin using nano alumina in aqueous medium, *Anal. Chem. Lett.* 10 (2) (2020) 227–239.
- [14] Y.A.R. Lebron, et al., Statistical physics modeling and optimization of norfloxacin adsorption onto graphene oxide, *Colloids Surf. A* 606 (2020) 125534.
- [15] N. Fang, et al., Toward broader applications of iron ore waste in pollution control: adsorption of norfloxacin, *J. Hazard. Mater.* 418 (2021) 126273.

- [16] M. Paredes-Laverde, J. Silva-Agrede, R.A. Torres-Palma, Removal of norfloxacin in deionized, municipal water and urine using rice (*Oryza sativa*) and coffee (*Coffea arabica*) husk wastes as natural adsorbents, *J. Environ. Manage.* 213 (2018) 98–108.
- [17] V.R. Moreira, et al., Graphene oxide in the remediation of norfloxacin from aqueous matrix: simultaneous adsorption and degradation process, *Environ. Sci. Pollut. Res. Int.* 27 (27) (2020) 34513–34528.
- [18] M.R. Azhar, et al., Adsorptive removal of antibiotic sulfonamide by UiO-66 and ZIF-67 for wastewater treatment, *J. Colloid Interface Sci.* 500 (2017) 88–95.
- [19] D.I. de Souza, et al., Nanofiltration for the removal of norfloxacin from pharmaceutical effluent, *J. Environ. Chem. Eng.* 6 (5) (2018) 6147–6153.
- [20] W. Liu, et al., Synergistic adsorption-photocatalytic degradation effect and norfloxacin mechanism of ZnO/ZnS@ BC under UV-light irradiation, *Sci. Rep.* 10 (1) (2020) 1–12.
- [21] J. He, et al., Understanding and characteristics of coagulation removal of composite pollution of microplastic and norfloxacin during water treatment, *Sci. Total Environ.* 831 (2022) 154826.
- [22] D. Balarak, et al., Survey electrocoagulation process in removal of norfloxacin antibiotic from aqueous solutions, *J. Pharmaceutical Res. Int.* 32 (3) (2020) 53–60.
- [23] W. Baran, et al., Removal of veterinary antibiotics from wastewater by electrocoagulation, *Chemosphere* 194 (2018) 381–389.
- [24] M. Bajpai, et al., A review on electrocoagulation process for the removal of emerging contaminants: theory, fundamentals, and applications, *Environ. Sci. Pollut. Res. Int.* 29 (2022) 1–30.
- [25] Y. Tian, et al., OD/3D coupling of g-C₃N₄ QDs/hierarchical macro-mesoporous CuO-SiO₂ for high-efficiency norfloxacin removal in photo-Fenton-like processes, *J. Hazard. Mater.* 419 (2021) 126359.
- [26] D. Yu, et al., Mineralization of norfloxacin in a CoFe-LDH/CF cathode-based heterogeneous electro-fenton system: preparation parameter optimization of the cathode and conversion mechanisms of H₂O₂ to ·OH, *Chem. Eng. J.* 417 (2021) 129240.
- [27] S.L. Prabavathi, et al., Construction of heterostructure CoWO₄/g-C₃N₄ nanocomposite as an efficient visible-light photocatalyst for norfloxacin degradation, *J. Ind. Eng. Chem.* 80 (2019) 558–567.
- [28] H. Zhang, et al., Preparation of Ce⁴⁺-doped BaZrO₃ by hydrothermal method and application in dual-frequent sonocatalytic degradation of norfloxacin in aqueous solution, *Ultrason. Sonochem.* 42 (2018) 356–367.
- [29] Y. Pan, et al., Norfloxacin pollution alters species composition and stability of plankton communities, *J. Hazard. Mater.* 385 (2020) 121625.
- [30] L. Wan, et al., Effect of norfloxacin on algae–cladoceran grazer–larval damselfly food chains: algal morphology-mediated trophic cascades, *Chemosphere* 256 (2020) 127166.
- [31] Y. Pan, et al., Lethal/sublethal responses of *Daphnia magna* to acute norfloxacin contamination and changes in phytoplankton-zooplankton interactions induced by this antibiotic, *Sci. Rep.* 7 (1) (2017) 1–10.
- [32] X. Liang, et al., Effects of norfloxacin nicotinate on the early life stage of zebrafish (*Danio rerio*): developmental toxicity, oxidative stress and immunotoxicity, *Fish Shellfish Immunol.* 96 (2020) 262–269.
- [33] X. Peng, et al., Amine-functionalized magnetic bamboo-based activated carbon adsorptive removal of ciprofloxacin and norfloxacin: a batch and fixed-bed column study, *Bioresour. Technol.* 249 (2018) 924–934.
- [34] V. Sharma, et al., Integrated adsorption-membrane filtration process for antibiotic removal from aqueous solution, *Powder Technol.* 321 (2017) 259–269.
- [35] H. Wu, et al., Retentions of bisphenol A and norfloxacin by three different ultrafiltration membranes in regard to drinking water treatment, *Chem. Eng. J.* 294 (2016) 410–416.
- [36] D. Dolar, et al., Photolysis of enrofloxacin and removal of its photodegradation products from water by reverse osmosis and nanofiltration membranes, *Sep. Purif. Technol.* 115 (2013) 1–8.
- [37] S.N. Oba, et al., Removal of ibuprofen from aqueous media by adsorption: a comprehensive review, *Sci. Total Environ.* 780 (2021) 146608.
- [38] C.A. Igwegbe, et al., Adsorption of ciprofloxacin from water: a comprehensive review, *J. Ind. Eng. Chem.* 93 (2021) 57–77.
- [39] M. Lippi, et al., State of art of landfill leachate treatment: literature review and critical evaluation, *Ciência e Natura* (2018) e78.
- [40] J. Mora-Gómez, et al., Electrochemical degradation of norfloxacin using BDD and new Sb-doped SnO₂ ceramic anodes in an electrochemical reactor in the presence and absence of a cation-exchange membrane, *Sep. Purif. Technol.* 208 (2019) 68–75.
- [41] G. Shankaraiah, et al., Degradation of antibiotic norfloxacin in aqueous solution using advanced oxidation processes (AOPs)—a comparative study, *Desalination Water Treat.* 57 (57) (2016) 27804–27815.
- [42] M. Bartolomeu, et al., Wastewater chemical contaminants: remediation by advanced oxidation processes, *Photochem. Photobiol. Sci.* 17 (11) (2018) 1573–1598.
- [43] E.A. Serna-Galvis, et al., Degradation of seventeen contaminants of emerging concern in municipal wastewater effluents by sonochemical advanced oxidation processes, *Water Res.* 154 (2019) 349–360.
- [44] S. Matavos-Aramyan, M. Moussavi, Advances in Fenton and Fenton based oxidation processes for industrial effluent contaminants control—a review, *Int. J. Environ. Sci. Nat. Resources* 2 (4) (2017) 1–18.
- [45] M.D. Klavarioti, et al., Removal of residual pharmaceuticals from aqueous systems by advanced oxidation processes, *Environ. Int.* 35 (2) (2009) 402–417.
- [46] J. Li, et al., Fabrication of FeVO₄/Fe₂TiO₅ composite catalyst and photocatalytic removal of norfloxacin, *Chem. Eng. J.* 298 (2016) 300–308.
- [47] P. García-Muñoz, et al., Evaluation of photoassisted treatments for norfloxacin removal in water using mesoporous Fe₂O₃-TiO₂ materials, *J. Environ. Manage.* 238 (2019) 243–250.
- [48] S. Ahmadi, et al., Sono electro-chemical synthesis of LaFeO₃ nanoparticles for the removal of fluoride: optimization and modeling using RSM, ANN and GA tools, *J. Environ. Chem. Eng.* 9 (4) (2021) 105320.
- [49] W. Liao, et al., Microwave-enhanced photolysis of norfloxacin: kinetics, matrix effects, and degradation pathways, *Int. J. Environ. Res. Public Health* 14 (12) (2017) 1564.
- [50] L.V. de Souza Santos, A.M. Meireles, L.C. Lange, Degradation of antibiotics norfloxacin by Fenton, UV and UV/H₂O₂, *J. Environ. Manage.* 154 (2015) 8–12.
- [51] J. Lu, et al., Kinetics, structural effects and transformation pathways for norfloxacin oxidation using the UV/chlorine process, *J. Water Process. Eng.* 44 (2021) 102324.
- [52] R. Su, et al., Chlorine dioxide radicals triggered by chlorite under visible-light irradiation for enhanced degradation and detoxification of norfloxacin antibiotic: radical mechanism and toxicity evaluation, *Chem. Eng. J.* 414 (2021) 128768.
- [53] J. Carrillo-Abad, et al., Effect of the CuO addition on a Sb-doped SnO₂ ceramic electrode applied to the removal of Norfloxacin in chloride media by electro-oxidation, *Chemosphere* 249 (2020) 126178.
- [54] H. Wang, et al., pH-dependent norfloxacin degradation by E⁺-ozonation: radical reactivities and intermediates identification, *J. Clean. Prod.* 265 (2020) 121722.
- [55] W. Chen, et al., Synthesis of MnOx/SBA-15 for Norfloxacin degradation by catalytic ozonation, *Sep. Purif. Technol.* 173 (2017) 99–104.
- [56] H. Chen, et al., Catalytic ozonation of norfloxacin using Co₃O₄/C composite derived from ZIF-67 as catalyst, *Chemosphere* 265 (2021) 129047.
- [57] X. Ma, et al., Ultrasound-enhanced nanosized zero-valent copper activation of hydrogen peroxide for the degradation of norfloxacin, *Ultrason. Sonochem.* 40 (2018) 763–772.
- [58] S.-B. Hu, et al., Aqueous norfloxacin sonocatalytic degradation with multilayer flower-like ZnO in the presence of peroxydisulfate, *Ultrason. Sonochem.* 38 (2017) 446–454.
- [59] A. Özcan, A.A. Özcan, Y. Demirci, Evaluation of mineralization kinetics and pathway of norfloxacin removal from water by electro-Fenton treatment, *Chem. Eng. J.* 304 (2016) 518–526.
- [60] G. Wang, et al., Removal of norfloxacin by surface Fenton system (MnFe₂O₄/H₂O₂): kinetics, mechanism and degradation pathway, *Chem. Eng. J.* 351 (2018) 747–755.
- [61] Q. Zhao, C.-C. Wang, P. Wang, Effective norfloxacin elimination via photo-Fenton process over the MIL-101 (Fe)-NH₂ immobilized on α-Al₂O₃ shee, *Chin. Chem. Lett.* 33 (11) (2022) 4828–4833.
- [62] Y. Wang, et al., Bio-Electron-Fenton (BEF) process driven by sediment microbial fuel cells (SMFCs) for antibiotics desorption and degradation, *Biosens. Bioelectron.* 136 (2019) 8–15.

- [63] G. Crini, E. Lichtfouse, Advantages and disadvantages of techniques used for wastewater treatment, *Environ. Chem. Lett.* 17 (1) (2019) 145–155.
- [64] J.T. Nwabanne, C.C. Obi, Coagulation-flocculation performance of snail shell biomass in abattoir wastewater treatment, *J. Chem. Technol. Metallurgy* 54 (6) (2019).
- [65] J.T. Nwabanne, C.C. Obi, Abattoir wastewater treatment by electrocoagulation using iron electrodes, *Chem. Sin.* 8 (2) (2017) 254–260.
- [66] J. Nwabanne, C.C. Obi, Electrocoagulation treatment of abattoirwastewater using aluminium electrode pairs, *NSChE J.* 33 (1) (2018) 65.
- [67] C.C. Obi, et al., Multi-characteristic optimization and modeling analysis of electrocoagulation treatment of abattoir wastewater using iron electrode pairs, *J. Water Process. Eng.* 49 (2022) 103136.
- [68] C.A. Igwegbe, O.D. Onukwuli, P.C. Onyechi, Optimal Route for Turbidity removal from Aquaculture Wastewater by Electrocoagulation-flocculation process, *J. Eng. Appl. Sci.* 15 (1) (2019) 99–108.
- [69] L.V. de Souza Santos, et al., Evaluation of the aerobic and anaerobic biodegradability of the antibiotic norfloxacin, *Water Sci. Technol.* 70 (2) (2014) 265–271.
- [70] B.S. Ondon, et al., Simultaneous removal and high tolerance of norfloxacin with electricity generation in microbial fuel cell and its antibiotic resistance genes quantification, *Bioresour. Technol.* 304 (2020) 122984.
- [71] R. Zhao, et al., Efficient enzymatic degradation used as pre-stage treatment for norfloxacin removal by activated sludge, *Bioprocess. Biosyst. Eng.* 40 (8) (2017) 1261–1270.
- [72] G. Wang, et al., Efficient removal of norfloxacin by biological aerated filters: effect of zeolite modification and analysis of microbial communities, *J. Water Process. Eng.* 40 (2021) 101799.
- [73] O.C. Iheanacho, et al., Packed bed column adsorption of phenol onto corn cob activated carbon: linear and nonlinear kinetics modeling, *S. Afr. J. Chem. Eng.* 36 (2021) 80–93.
- [74] J.T. Nwabanne, et al., Linear and nonlinear kinetics analysis and adsorption characteristics of packed bed column for phenol removal using rice husk-activated carbon, *Appl. Water Sci.* 12 (5) (2022) 1–16.
- [75] C. Igwegbe, et al., Studies on adsorption characteristics of corn cobs activated carbon for the removal of oil and grease from oil refinery desalter effluent in a downflow fixed bed adsorption equipment, *Eur. J. Sustainable Dev. Res.* 5 (1) (2020).
- [76] C.A. Igwegbe, et al., Equilibrium and kinetics analysis on vat yellow 4 uptake from aqueous environment by modified rubber seed shells: nonlinear modelling, *J. Mater. Environ. Sci.* 11 (9) (2020) 1424–1444.
- [77] T. Qin, et al., A novel biochar derived from cauliflower (*Brassica oleracea* L.) roots could remove norfloxacin and chlortetracycline efficiently, *Water Sci. Technol.* 76 (12) (2017) 3307–3318.
- [78] B. Wang, et al., Preparation of biochar by simultaneous carbonization, magnetization and activation for norfloxacin removal in water, *Bioresour. Technol.* 233 (2017) 159–165.
- [79] Y. Luo, et al., CuNiN@ C coupled with peroxymonosulfate as efficient catalytic system for the removal of norfloxacin by adsorption and catalysis, *Sep. Purif. Technol.* 252 (2020) 117476.
- [80] Y. Wan, et al., Optimization adsorption of norfloxacin onto polydopamine microspheres from aqueous solution: kinetic, equilibrium and adsorption mechanism studies, *Sci. Total Environ.* 639 (2018) 428–437.
- [81] B. Tegegne, et al., Molecularly imprinted polymer for adsorption of venlafaxine, albendazole, ciprofloxacin and norfloxacin in aqueous environment, *Sep. Sci. Technol.* 56 (13) (2021) 2217–2231.
- [82] F. Jing, et al., Mechanistic insight into adsorptive removal of ionic NOR and nonionic DEP organic contaminants by clay-biochar composites, *Environ. Pollut.* 310 (2022) 119881.
- [83] N.A. Khan, et al., Efficient removal of norfloxacin by MOF@ GO composite: isothermal, kinetic, statistical, and mechanistic study, *Toxin Rev.* 40 (4) (2021) 915–927.
- [84] F. Zhu, et al., Degradation mechanism of norfloxacin in water using persulfate activated by BC@ nZVI/Ni, *Chem. Eng. J.* 389 (2020) 124276.
- [85] L. Fang, et al., Efficient removal of norfloxacin in water using magnetic molecularly imprinted polymer, *Chemosphere* 262 (2021) 128032.
- [86] X. Wu, et al., Recognizing removal of norfloxacin by novel magnetic molecularly imprinted chitosan/ γ -Fe₂O₃ composites: selective adsorption mechanisms, practical application and regeneration, *Sep. Purif. Technol.* 165 (2016) 92–100.
- [87] K.O. Iwuozor, et al., Aqueous phase adsorption of aromatic organoarsenic compounds: a review, *J. Water Process. Eng.* 49 (2022) 103059.
- [88] J.O. Ighalo, et al., Utilisation of adsorption as a resource recovery technique for lithium in geothermal water, *J. Mol. Liq.* (2022) 120107.
- [89] Z. Wang, et al., Loofah activated carbon with hierarchical structures for high-efficiency adsorption of multi-level antibiotic pollutants, *Appl. Surf. Sci.* 550 (2021) 149313.
- [90] B. Yan, C.H. Niu, J. Wang, Kinetics, electron-donor-acceptor interactions, and site energy distribution analyses of norfloxacin adsorption on pretreated barley straw, *Chem. Eng. J.* 330 (2017) 1211–1221.
- [91] D. Chen, et al., MOF-derived magnetic porous carbon-based sorbent: synthesis, characterization, and adsorption behavior of organic micropollutants, *Adv. Powder Technol.* 28 (7) (2017) 1769–1779.
- [92] M. Nazraz, Y. Yamini, H. Asiabi, Chitosan-based sorbent for efficient removal and extraction of ciprofloxacin and norfloxacin from aqueous solutions, *Microchim. Acta* 186 (7) (2019) 1–9.
- [93] J.O. Ighalo, et al., Cost of adsorbent preparation and usage in wastewater treatment: a review, *Cleaner Chem. Eng.* 3 (2022) 100042.
- [94] K.O. Iwuozor, et al., An empirical literature analysis of adsorbent performance for methylene blue uptake from aqueous media, *J. Environ. Chem. Eng.* 9 (4) (2021) 105658.
- [95] J.O. Ighalo, et al., Verification of pore size effect on aqueous-phase adsorption kinetics: a case study of methylene blue, *Colloids Surf. A* 626 (2021) 127119.
- [96] J.O. Ighalo, et al., A review of pine-based adsorbents for the adsorption of dyes, *Biomass-Derived Mater. Environ. Appl.* (2022) 319–332.
- [97] K.O. Iwuozor, et al., Do adsorbent pore size and specific surface area affect the kinetics of methyl orange aqueous phase adsorption? *J. Chem. Lett.* 4 (2021) 11.
- [98] B.L.G.L. Zanli, W. Tang, J. Chen, N-doped and activated porous biochar derived from cocoa shell for removing norfloxacin from aqueous solution: performance assessment and mechanism insight, *Environ. Res.* 214 (3) (2022) 113951.
- [99] X. Guo, et al., Exploration of functional MOFs for efficient removal of fluoroquinolone antibiotics from water, *Microporous Mesoporous Mater.* 286 (2019) 84–91.
- [100] J. Zhang, et al., Effects of pH, dissolved humic acid and Cu²⁺ on the adsorption of norfloxacin on montmorillonite-biochar composite derived from wheat straw, *Biochem. Eng. J.* 130 (2018) 104–112.
- [101] W. Chen, et al., Efficient adsorption of Norfloxacin by Fe-MCM-41 molecular sieves: kinetic, isotherm and thermodynamic studies, *Chem. Eng. J.* 281 (2015) 397–403.
- [102] X. Niu, et al., High specific surface area N-doped activated carbon from hydrothermal carbonization of shaddock peel for the removal of norfloxacin from aqueous solution, *Water Sci. Technol.* 85 (10) (2022) 2964–2979.
- [103] Q. Liu, et al., Green synthesis of stable Fe, Cu oxide nanocomposites from loquat leaf extracts for removal of Norfloxacin and Ciprofloxacin, *Water Sci. Technol.* 81 (4) (2020) 694–708.
- [104] J. Wang, et al., Adsorption characteristics and mechanism of norfloxacin in water by γ -Fe₂O₃@ BC, *Water Sci. Technol.* 82 (2) (2020) 242–254.
- [105] K.O. Iwuozor, et al., A review on the mitigation of heavy metals from aqueous solution using sugarcane bagasse, *SugarTech* 23 (2021) 19.
- [106] J.O. Ighalo, et al., Adsorption of persistent organic pollutants (POPs) from the aqueous environment by nano-adsorbents: a review, *Environ. Res.* 212 (2022) 113123.
- [107] H. Xie, et al., Sorption of norfloxacin from aqueous solutions by activated carbon developed from *Trapa natans* husk, *Sci. China Chem.* 54 (5) (2011) 835–843.
- [108] P. Ma, et al., Green synthesis of Fe/Cu oxides composite particles stabilized by pine needle extract and investigation of their adsorption activity for norfloxacin and ofloxacin, *J. Dispers. Sci. Technol.* 42 (9) (2021) 1350–1367.

- [109] G. Li, et al., Bifunctional monomer molecularly imprinted sol-gel polymers based on the surface of magnetic halloysite nanotubes as an effective extraction approach for norfloxacin, *Appl. Clay Sci.* 162 (2018) 409–417.
- [110] W. Liu, et al., Sorption of norfloxacin by lotus stalk-based activated carbon and iron-doped activated alumina: mechanisms, isotherms and kinetics, *Chem. Eng. J.* 171 (2) (2011) 431–438.
- [111] B. Yan, C.H. Niu, Adsorption behavior of norfloxacin and site energy distribution based on the Dubinin-Astakhov isotherm, *Sci. Total Environ.* 631 (2018) 1525–1533.
- [112] Y. Zhou, et al., Simultaneous removal of tetracycline and norfloxacin from water by iron-trimesic metal-organic frameworks, *J. Environ. Chem. Eng.* 10 (3) (2022) 107403.
- [113] H. Liu, et al., Evaluation of animal hairs-based activated carbon for sorption of norfloxacin and acetaminophen by comparing with cattail fiber-based activated carbon, *J. Anal. Appl. Pyrolysis* 101 (2013) 156–165.
- [114] C. Li, et al., Synergistic effects of anionic surfactants on adsorption of norfloxacin by magnetic biochar derived from furfural residue, *Environ. Pollut.* 254 (2019) 113005.
- [115] J.-R. Li, et al., Can adsorbent of layered chalcogenide be regenerated? A case study of norfloxacin adsorbed by layered chalcogenide in water, *Colloids Surf. A* 537 (2018) 287–293.
- [116] M.E. Zelaya Soulé, et al., Norfloxacin adsorption on montmorillonite and carbon/montmorillonite hybrids: pH effects on the adsorption mechanism, and column assays, *J. Environ. Sci. Health, Part A* 56 (1) (2020) 113–122.
- [117] Y. Xu, et al., Crystal engineering of novel MOF@ iCOF composite as a multifunction platform for targeted monitoring and capturing of norfloxacin, *Chem. Eng. J.* 435 (2022) 134907.
- [118] H. Dan, et al., Mechanism of sonication time on structure and adsorption properties of 3D peanut shell/graphene oxide aerogel, *Sci. Total Environ.* 739 (2020) 139983.
- [119] Y. Hu, et al., Surface-imprinted polymer microsphere based on self-stabilized precipitation polymerization for selective removal of norfloxacin, *Appl. Surf. Sci.* 574 (2022) 151706.
- [120] P. Liu, et al., Preparation of magnetic biochar obtained from one-step pyrolysis of *Salix mongolica* and investigation into adsorption behavior of sulfadiazine sodium and norfloxacin in aqueous solution, *J. Dispers. Sci. Technol.* 41 (2) (2020) 214–226.
- [121] W. Yang, et al., Adsorption behavior and mechanisms of norfloxacin onto porous resins and carbon nanotube, *Chem. Eng. J.* 179 (2012) 112–118.
- [122] J. Chen, et al., Comparison of adsorption characteristics of acid-base modified fly ash to norfloxacin, *Spectrosc. Lett.* 53 (6) (2020) 416–429.
- [123] M.J. Ahmed, S.K. Theydan, Fluoroquinolones antibiotics adsorption onto microporous activated carbon from lignocellulosic biomass by microwave pyrolysis, *J. Taiwan Inst. Chem. Eng.* 45 (1) (2014) 219–226.
- [124] P. Liu, et al., Sorption of sulfadiazine, norfloxacin, metronidazole, and tetracycline by granular activated carbon: kinetics, mechanisms, and isotherms, *Water Air Soil Pollut.* 228 (4) (2017) 1–14.
- [125] L. Yi, et al., Rapid nitrogen-rich modification of *Calotropis gigantea* fiber for highly efficient removal of fluoroquinolone antibiotics, *J. Mol. Liq.* 256 (2018) 408–415.
- [126] Prarat, P., et al., Removal of norfloxacin antibiotic from aqueous solution by activated carbon prepared from pomelo peel biomass waste by chemical activation. *Environ. Asia*, 2020. 13.
- [127] Z. Qiu, et al., Regenerable Mg/Fe bimetallic hydroxide for remarkable removal of low-concentration norfloxacin from aqueous solution, *Colloids Surf. A* 644 (2022) 128825.
- [128] G. Che, et al., Unraveling influence of metal species on norfloxacin removal by mesoporous metallic silicon adsorbent, *Environ. Sci. Pollut. Res. Int.* 27 (28) (2020) 35638–35649.
- [129] V.-T. Nguyen, et al., Adsorption of norfloxacin from aqueous solution on biochar derived from spent coffee ground: master variables and response surface method optimized adsorption process, *Chemosphere* 288 (2022) 132577.
- [130] J.O. Otalvaro, M. Avena, M. Brigante, Adsorption of norfloxacin on a hexagonal mesoporous silica: isotherms, kinetics and adsorbent reuse, *Adsorption* 25 (7) (2019) 1375–1385.
- [131] S. Zhao, et al., Microwave-assisted hydrothermal assembly of 2D copper-porphyrin metal-organic frameworks for the removal of dyes and antibiotics from water, *Environ. Sci. Pollut. Res. Int.* 27 (31) (2020) 39186–39197.
- [132] M.M. Gaho, et al., Synthesis of novel magnetic molecularly imprinted polymers by solid-phase extraction method for removal of norfloxacin, *Chin. J. Anal. Chem.* 50 (6) (2022) 100079.
- [133] Y. Ma, et al., Iron/zinc and phosphoric acid modified sludge biochar as an efficient adsorbent for fluoroquinolones antibiotics removal, *Ecotoxicol. Environ. Saf.* 196 (2020) 110550.
- [134] Y. Tang, et al., Synthesis of reduced graphene oxide/magnetite composites and investigation of their adsorption performance of fluoroquinolone antibiotics, *Colloids Surf. A* 424 (2013) 74–80.
- [135] J. Wu, et al., Norfloxacin adsorption and subsequent degradation on ball-milling tailored N-doped biochar, *Chemosphere* (2022) 135264.
- [136] M. Sui, et al., Adsorption of norfloxacin in aqueous solution by Mg–Al layered double hydroxides with variable metal composition and interlayer anions, *Chem. Eng. J.* 210 (2012) 451–460.
- [137] M. Zhang, et al., Study on optimal adsorption conditions of norfloxacin in water based on response surface methodology, *Water Supply* 22 (4) (2022) 3661–3672.
- [138] R. Li, et al., Magnetic biochar-based manganese oxide composite for enhanced fluoroquinolone antibiotic removal from water, *Environ. Sci. Pollut. Res. Int.* 25 (31) (2018) 31136–31148.
- [139] X. Yang, et al., Mechanistic insights into removal of norfloxacin from water using different natural iron ore–biochar composites: more rich free radicals derived from natural pyrite–biochar composites than hematite–biochar composites, *Appl. Catal. B* 255 (2019) 117752.
- [140] D. Qin, et al., Selective extraction and detection of norfloxacin from marine sediment and seawater samples using molecularly imprinted silica sorbents coupled with HPLC, *Mar. Pollut. Bull.* 150 (2020) 110677.
- [141] R.A. Wuana, R. Sha'Ato, S. Iorhen, Preparation, characterization, and evaluation of *Moringa oleifera* pod husk adsorbents for aqueous phase removal of norfloxacin, *Desalination Water Treat.* 57 (25) (2016) 11904–11916.
- [142] Z. Liang, et al., Adsorption of quinolone antibiotics in spherical mesoporous silica: effects of the retained template and its alkyl chain length, *J. Hazard. Mater.* 305 (2016) 8–14.
- [143] K.O. Iwuozor, et al., Mitigation of levofloxacin from aqueous media by adsorption: a review, *Sustain. Water Resour. Manag.* 7 (6) (2021) 1–18.
- [144] E.C. Emenike, et al., Recent advances in nano-adsorbents for the sequestration of copper from water, *J. Water Process. Eng.* 47 (2022) 102715.
- [145] H. Peng, et al., Adsorption of ofloxacin and norfloxacin on carbon nanotubes: hydrophobicity-and structure-controlled process, *J. Hazard. Mater.* 233 (2012) 89–96.
- [146] X. Li, et al., Modified activated carbon fiber felt for the electrosorption of norfloxacin in aqueous solution, *Sustainability* 12 (10) (2020) 3986.
- [147] L. Zhou, et al., Simultaneous removal of mixed contaminants, copper and norfloxacin, from aqueous solution by ZIF-8, *Chem. Eng. J.* 362 (2019) 628–637.
- [148] C.A. Igwegbe, et al., Electrocoagulation-flocculation of aquaculture effluent using hybrid iron and aluminium electrodes: a comparative study, *Chem. Eng. J. Adv.* 6 (2021) 100107.
- [149] C.E. Barquilha, M.C. Braga, Adsorption of organic and inorganic pollutants onto biochars: challenges, operating conditions, and mechanisms, *Bioresour. Technol. Rep.* 15 (2021) 100728.
- [150] K. Roy, et al., Background of QSAR and historical developments, *Understanding the Basics of QSAR For Applications in Pharmaceutical Sciences and Risk Assessment*, 1st edn., Academic, London, 2015.
- [151] T. Ambaye, et al., Mechanisms and adsorption capacities of biochar for the removal of organic and inorganic pollutants from industrial wastewater, *Int. J. Environ. Sci. Technol.* 18 (10) (2021) 3273–3294.

- [152] C.E. Onu, et al., Decolorization of bromocresol green dye solution by acid functionalized rice husk: artificial intelligence modeling, GA optimization, and adsorption studies, *J. Hazard Mater. Adv.* 9 (2023) 1–14.
- [153] E.C. Emenike, et al., Efficient recycling of disposable face masks via co-carbonization with waste biomass: a pathway to a cleaner environment, *Clean. Environ. Syst.* (2022) 100094.
- [154] O. Lorphensri, et al., Sorption of acetaminophen, 17 α -ethynyl estradiol, nalidixic acid, and norfloxacin to silica, alumina, and a hydrophobic medium, *Water Res.* 40 (7) (2006) 1481–1491.
- [155] Y. Chen, Z. Li, Interaction of norfloxacin and hexavalent chromium with ferrihydrite nanoparticles: synergistic adsorption and antagonistic aggregation behavior, *Chemosphere* 299 (2022) 134386.
- [156] Z.-G. Pei, et al., Insight to ternary complexes of co-adsorption of norfloxacin and Cu (II) onto montmorillonite at different pH using EXAFS, *J. Hazard. Mater.* 186 (1) (2011) 842–848.
- [157] J. Luo, et al., Sorption of norfloxacin, sulfamerazine and oxytetracycline by KOH-modified biochar under single and ternary systems, *Bioresour. Technol.* 263 (2018) 385–392.
- [158] N. Yao, et al., Norfloxacin and bisphenol-A removal using temperature-switchable graphene oxide, *ACS Appl. Mater. Interfaces* 10 (34) (2018) 29083–29091.
- [159] D. Feng, et al., Adsorption characteristics of norfloxacin by biochar prepared by cassava dreg: kinetics, isotherms, and thermodynamic analysis, *Bioresources* 10 (4) (2015) 6751–6768.
- [160] L. Zhao, et al., Sorption of copper and norfloxacin onto humic acid: effects of pH, ionic strength, and foreign ions, *Environ. Sci. Pollut. Res. Int.* 26 (11) (2019) 10685–10694.
- [161] E.C. Emenike, et al., Delonix regia biochar potential in removing phenol from industrial wastewater, *Bioresour. Technol. Rep.* (2022) 101195.
- [162] O. Ogundalu, et al., Trends in the mitigation of heavy metal ions from aqueous solutions using unmodified and chemically-modified agricultural waste adsorbents, *Curr. Res. Green Sustainable Chem.* 4 (2021) 100188.
- [163] E.C. Emenike, K.O. Iwuozor, S.U. Anidiobi, Heavy metal pollution in aquaculture: sources, impacts and mitigation techniques, *Biol. Trace Elem. Res.* 200 (2021) 1–17.
- [164] O. Bunkoed, P. Donkhampa, P. Nurerk, A nanocomposite optosensor of hydroxyapatite and graphene quantum dots embedded within highly specific polymer for norfloxacin detection, *Microchem. J.* 158 (2020) 105127.
- [165] A.M. Aibinu, et al., Green synthesis of CuO nanocomposite from watermelon (*Citrullus lanatus*) rind for the treatment of aquaculture effluent, *Reg. Stud. Marine Sci.* 52 (2022) 102308.
- [166] K.O. Iwuozor, et al., Removal of pollutants from aqueous media using cow dung-based adsorbents, *Curr. Res. Green Sustainable Chem.* 5 (2022) 100300.
- [167] K.O. Iwuozor, et al., Adsorption of organophosphate pesticides from aqueous solution: a review of recent advances, *Int. J. Environ. Sci. Technol.* (2022) **In press**.
- [168] T.M. Darweesh, M.J. Ahmed, Adsorption of ciprofloxacin and norfloxacin from aqueous solution onto granular activated carbon in fixed bed column, *Ecotoxicol. Environ. Saf.* 138 (2017) 139–145.
- [169] Q. Hu, et al., Prediction of breakthrough curves in a fixed-bed column based on normalized Gudermannian and error functions, *J. Mol. Liq.* 323 (2021) 115061.
- [170] J.O. Ighalo, et al., Utilization of avocado (*Persea americana*) adsorbents for the elimination of pollutants from water: a review, *Biomass-Der. Mater. Environ. Appl.* (2022) 333–348.
- [171] T.T. Firozjaee, et al., The removal of diazinon from aqueous solution by chitosan/carbon nanotube adsorbent, *Desalin. Water Treat.* 79 (2017) 291–300.
- [172] J. Ighalo, et al., Recent advances in hydrochar application for the adsorptive removal of wastewater pollutants, *Chem. Eng. Res. Des.* 184 (2022) 38.
- [173] S. Li, L. Fang, Modeling of the adsorption mechanisms and selectivity of the molecular imprinted particles for norfloxacin, *Advanced Materials Research*, 2014 Trans Tech Publ.
- [174] Y. Zhang, L. Cheng, Y. Ji, A novel amorphous porous biochar for adsorption of antibiotics: adsorption mechanism analysis via experiment coupled with theoretical calculations, *Chem. Eng. Res. Des.* 186 (2022) 362–373.
- [175] S. Yadav, et al., Removal of fluoroquinolone from aqueous solution using graphene oxide: experimental and computational elucidation, *Environ. Sci. Pollut. Res. Int.* 25 (3) (2018) 2942–2957.
- [176] X. Zhang, et al., Interactions between antibiotics and graphene-based materials in water: a comparative experimental and theoretical investigation, *ACS Appl. Mater. Interfaces* 8 (36) (2016) 24273–24280.
- [177] R. Guo, K. Lin, Y. Ai, Insights into the interface mechanism of three typical antibiotics onto the graphene oxide/chitosan composite: an experimental and theoretical investigation, *Chin. J. Chem. Phys.* (2021).
- [178] D. Liang, et al., Design, preparation and adsorption performances of norfloxacin molecularly imprinted polymers, *J. Mol. Graphics Modell.* 114 (2022) 108197.
- [179] J.O. Ighalo, et al., Mitigation of metronidazole (flagyl) pollution in aqueous media by adsorption: a review, *Environ. Technol. Rev.* 9 (1) (2020) 137–148.
- [180] P.E. Ohale, et al., Adsorptive kinetics, isotherm and thermodynamic analysis of fishpond effluent coagulation using chitin derived coagulant from waste *Brachyura* shell, *Chem. Eng. J. Adv.* 4 (2020) 100036.
- [181] H.N. Tran, et al., Mistakes and inconsistencies regarding adsorption of contaminants from aqueous solutions: a critical review, *Water Res.* 120 (2017) 88–116.
- [182] J. Bednárek, et al., Revelation of high-adsorption-performance activated carbon for removal of fluoroquinolone antibiotics from water, *Biomass Convers. Biorefin.* (2022) 1–15.
- [183] M. Xi, et al., Enhanced norfloxacin degradation by iron and nitrogen co-doped biochar: revealing the radical and nonradical co-dominant mechanism of persulfate activation, *Chem. Eng. J.* 420 (2021) 129902.
- [184] W. Huang, et al., Preparation and characterization of novel thermosensitive magnetic molecularly imprinted polymers for selective recognition of norfloxacin, *J. Polym. Res.* 23 (5) (2016) 1–11.
- [185] P.E. Ohale, et al., A comparative optimization and modeling of ammonia–nitrogen adsorption from abattoir wastewater using a novel iron-functionalized crab shell, *Appl. Water Sci.* 12 (8) (2022) 1–27.
- [186] S. Chen, et al., Study on the adsorption of dyestuffs with different properties by sludge-rice husk biochar: adsorption capacity, isotherm, kinetic, thermodynamics and mechanism, *J. Mol. Liq.* 285 (2019) 62–74.
- [187] C. Aniaigor, M. Menkiti, Kinetics and mechanistic description of adsorptive uptake of crystal violet dye by lignified elephant grass complexed isolate, *J. Environ. Chem. Eng.* 6 (2) (2018) 2105–2118.